AN INVESTIGATION OF SERIES LC RESONANT CIRCUITS WITHIN A SLEEVE BALUN TO ACHIEVE WIDEBAND OPERATION

BY

CHRISTIE M. BERMUDEZ-RIVERA

THESIS

Submitted in partial fulfillment of the requirements
for the degree of Master of Science in Electrical and Computer Engineering
in the Graduate College of the
University of Illinois at Urbana-Champaign, 2014

Urbana, Illinois

Adviser:

Professor Jennifer T. Bernhard

ABSTRACT

In antenna measurements, it is not recommended to connect a balanced antenna directly to the coaxial cable feed. A balun is required to prevent surface current from flowing onto the outer shield of the feed cable. Balun chokes like the sleeve balun, also known as bazooka balun or quarter-wavelength balun, are commonly used in antenna measurements. In general, baluns do perform well, but their performance is band-limited. Hence, for wider frequency bands, multiple baluns with different operating frequencies have to be used. This presents a major problem, especially in broadband antenna measurements. To this end, a proposed design based on the quarter-wave bazooka (sleeve) balun has been investigated. The design consists of resonators arranged in a log-periodic manner. The main objective of this design is to have high impedance and therefore high common mode rejection ratios at different frequencies. To do so, resonant series LC circuits were placed between the outer shield of the coaxial cable and the inner wall of the balun. These are intended to create short circuit terminations within the balun at different design frequencies. Two models have been investigated: one with two LC circuits and the other with four LC circuits. The variables considered in the study included circuit placement and circuit quality factor Q. Simulations in Agilent ADS® and HFSS® 14.0 were performed to study the common mode rejection ratio (CMRR) parameter of the different proposed designs. In addition, three baluns were built and measured in order to compare with simulations. Results demonstrated that the Q of the inductor significantly affects the response over a frequency range. Comparisons of the performance of the different designs are presented in detail in this work. All designs achieved a common mode rejection ratio above 30 dB over a wideband frequency range.

To my parents, for their love and support during all these years

ACKNOWLEDGMENTS

I am profoundly grateful to my adviser, Professor Jennifer T. Bernhard, for her guidance, patience, and support. Today, I feel privileged to be part of her research group. Thank you for believing in me and thank you for giving me the opportunity to advance one more step in my professional career.

To my cousins Eric J. Correa and Alessandra Correa, who encouraged me to apply for the Summer Research Opportunity Program at the UIUC.

To my undergraduate professors, especially to Prof. Caroline Gonzalez-Rivera, who encouraged me to pursue graduate studies. She introduced me to the RF/communication world. I am very grateful to her for all the knowledge and counseling that she gave me during my academic years.

To the people I love most in my life, my parents, for their understanding and support of me at every stage of my life. They always have the right words at the right times. They encourage me to work hard, and to reach as far as I can go without losing the values of respect and humility. Most importantly, they taught me to always believe in myself and to have faith in God.

A special thanks to Rijan P. Shrestha for being my Guardian Angel during this journey. Thanks for being there for me when I needed you. I will always be grateful for all your support.

Christie Marie Bermúdez

TABLE OF CONTENTS

LIST OF FIGURES

CHAPTER 1

INTRODUCTION

1.1 Motivation

Accurate radiation patterns and input impedance measurements are important for successful antenna designs. For electrically small antennas, these characteristics can present significant challenges in measurements [1]. One area of active research is to explore ways to reduce cable loading effects on electrically small antennas. Antennas are either balanced or unbalanced, and hence should be fed accordingly to minimize the cable loading effects and attain reliable input impedance and radiation patterns [2]. However, these measurements are not easy to perform for balanced antennas, since the feed currents have to be equal and opposite in phase. Most network analyzers are terminated by unbalanced ports like coaxial cables [3]. When a coax is connected to a balanced load such as a dipole, a current may flow back on the outside of the outer conductor, which causes an imbalance in the antenna and transmission line. This unwanted current causes the feed line to act like an antenna, radiating a field that is proportional to this current. This results in antenna pattern distortion and changes in the input impedance at the cable input [4]. One of the most common ways of eliminating this problem is to use a balun. A balun is a balanced-to-unbalanced converter; when it is used in antenna measurements, it reduces unwanted cable current by balancing the antenna current. Over the years, many balun designs have been developed. Some of the balun designs also possess impedance transformation properties. Any desired impedance transformation can usually be accomplished using common design methods [5].

Baluns used for low-frequency ranges in antenna applications perform well in a narrow band frequency. As a result, in applications like wideband antenna measurements, different baluns are required. As the balun is already

larger than the antenna itself, especially in the case of electrically small antennas, using multiple baluns poses a constraint. This is a major problem in practice, especially in antenna measurement. This work investigates a log-periodic design using resonant series LC circuits placed between the outer shield of the coaxial cable and the inner wall of the balun. Two models have been investigated: one with two LC circuits and the other with four LC circuits. In order to understand why baluns are important in antenna measurements, the following sections present in more detail the concept of balanced and unbalanced lines and what happens when a dipole antenna is connected directly to a coaxial cable feed.

1.2 Balanced and Unbalanced Concept

A balanced line is defined as a transmission line with two identical conductors. The impedance of the line is constant along its length and to ground. Examples of balanced transmission lines are twin lead and twisted pairs. On the other hand, an unbalanced line has two conductors with unequal impedances with respect to ground. One conductor is considered as the signal line and the other as the grounded line. Microstrip lines and coaxial cables are examples of unbalanced transmission lines. A transmission line carrying differential signaling does not make the line balanced. Equivalently, a balanced line does not require differential signaling [5],[6].

The concept of balanced and unbalanced transmission lines is easy to understand if we think of the line in relation to a conducting plane as shown in Figure 1.1. The ground plane now becomes a third conductor. Currents in the conducting line now exist in the signal lines. In a balanced transmission line, capacitances of the two conductors to ground are the same; for an unbalanced line they are not. The inner conductor has no direct capacitance to ground [6],[7].

In general, a balanced line has the following characteristics. First, the voltage difference between the two conductors is the voltage propagating down the line. Second, both the conductors have some voltage with respect to ground. This voltage is called the common mode voltage. Last, the currents flow between the conductors due to common mode voltages.

For the unbalanced transmission line, the line connected to ground has

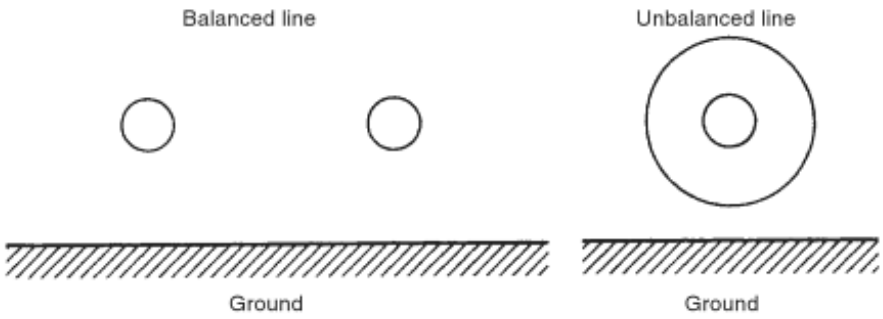

Figure 1.1: Balanced and unbalanced transmission lines [7]

infinite resistance. Hence a small voltage difference can exist between two points on a grounded line [7]. In addition, the signal propagating in the line can be measured as the voltage difference with respect to ground. There are no common mode signals on unbalanced lines [6].

It is also common to divide antennas into balanced and unbalanced antennas. Unbalanced antennas are also called single-ended antennas, while balanced antennas are often called differential antennas. A balanced antenna does not have a conductor connected directly to ground. The impedance between ground and each conductor is the same. Usually, a balanced antenna has characteristic impedance of 50 Ω. A folded dipole is a typical example of a balanced antenna. In contrast, an unbalanced antenna has one of its conductors connected to the earth. The impedances between the ground and each conductor are not the same. A monopole is an example of an unbalanced antenna [8].

1.3 Connecting a Balanced Load to an Unbalanced Line

Figure 1.2 shows what happens when a balanced line like a coaxial cable is connected to a balanced load like a half-wave dipole [9]. The half-wave dipole is a balanced and symmetrical structure that is fed at its center by a generator connected to the terminals. The current has symmetrical distribution with respect to the center and it is zero at the ends. This antenna performs best when the sides are fed with separate currents of equal amplitude and opposite

phase [10]. In contrast, a coaxial cable is an unbalanced feed line in which all the currents flow inside the line [4].

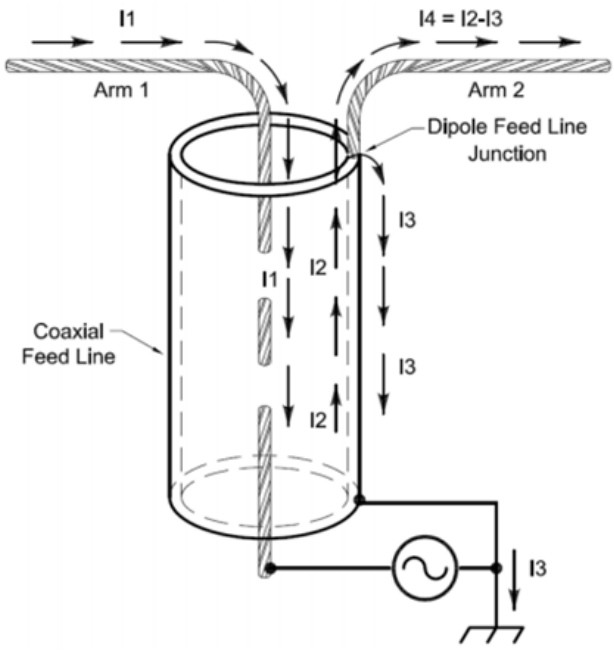

Figure 1.2: Coax cable connected directly to a dipole antenna [11]

Figure 1.2 shows a balanced antenna connected to a coaxial cable. A voltage is applied at the end of the cable across the antenna's terminal. At the antenna terminal the voltages will be equal in magnitude but opposite in phase. Both voltages will cause a current on the outside of the coaxial cable. Since one antenna terminal is connected directly to the outer conductor, the voltage produces a much stronger current than in the other terminal. In other words, the current that flows in the terminal connected to the outer conductor will split [10].

This situation can be represented in a circuit model. Capacitance between the arms of the dipole and the outer conductor of the coaxial are created due to the applied voltage as shown in Figure 1.3(a). Clearly one capacitance will be bigger than the other; therefore, the equivalent circuit has unequal impedances on either side. As result the system is unbalanced [12].

The antenna now has two different currents: the expected current and a current that represents the unwanted mode introduced by the feed method. This unwanted current will add radiation components to the antenna and will degrade the dipole pattern. In addition, this current will change the

Figure 1.3: (a) Stray capacitances at dipole antenna (b) The wanted radiating current mode (solid) and the unwanted current (dashed line) [12]

input impedance at the cable input. The unwanted current can be reduced by introducing a balun transformer between the terminals of the antenna and the coaxial feed cable [6], [12]. The common solution is to connect a quarter-wavelength sleeve to the feed cable, a device known as a sleeve balun, bazooka balun, or sleeve choke [9]. Ferrite beads can provide an alternative solution, but they are lossy at higher frequencies. Ferrite beads are not usually used in electrically small antennas because they reduce the gain of the antenna at the relevant frequency of operation [5].

Eggers in 1980 described the importance of using a bazooka balun in antenna measurements [13]. Figure 1.4 shows the response pattern of a half-wave dipole with and without the balun measured in the RF anechoic chamber. The peak amplitude of the pattern of the dipole without the balun is about 5 dB below that of the balun-fed antenna. In addition, the antenna beam is redirected as shown in Figure 1.4(b).

It is always recommended to use a balun between the feed cable and an antenna even if the antenna is an unbalanced one. Cables that carry RF currents or voltages are more likely to radiate if they are not connected to a balun. In the case of small unbalanced antennas, the current flowing on the outer conductor could be much greater than that in the balanced case [12]. Studies have shown that devices that are small in terms of wavelength are more susceptible to cable loading [6].

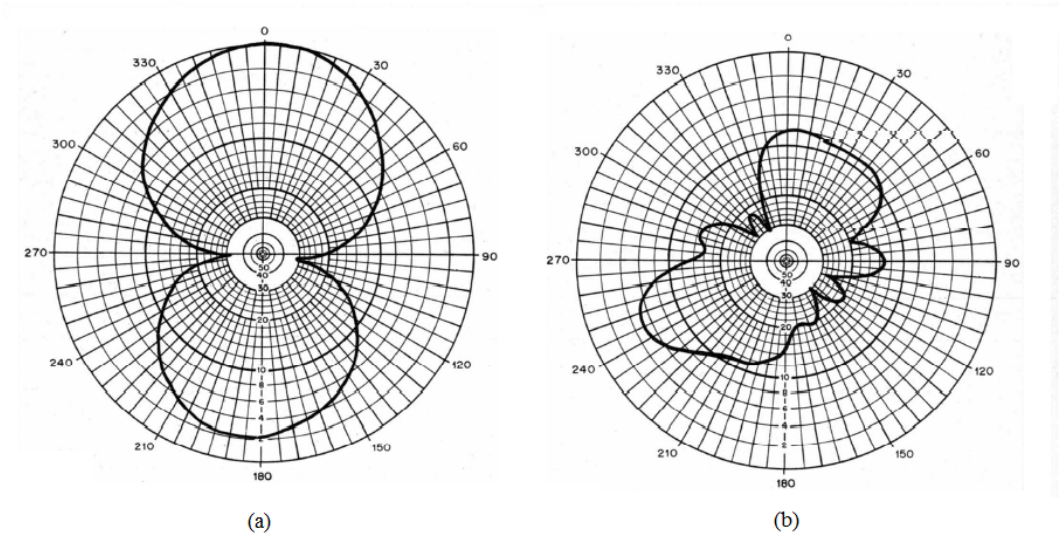

Figure 1.4: (a) Response pattern of the balun-fed half-wavelength dipole in RF anechoic chamber (b) Response of a half-wavelength dipole without a balun [13]

1.4 Overview

An outline of the structure of this thesis is presented in this section. Chapter 2 presents general information about baluns, focusing on baluns used in electrically small antennas. The performance of the bazooka sleeve balun and the folded balun will be discussed and supported by simulation made in HFSS®. Chapter 3 describes the proposed designs to achieved wide bandwidth. Simulated results and comparisons are also provided in this chapter. Chapter 4 presents the construction and measurement of three baluns. Finally, Chapter 5 summarizes the thesis and suggests future work for potential improvements.

CHAPTER 2

GENERAL BALUN THEORY

The balun has a long history. The word balun was first documented as a device to feed a television transmitting antenna for the Empire State Building in 1939 [14]. Baluns are found in a wide variety of applications, especially in wireless and RF applications. Baluns can be found in circuits such as mixers, amplifiers, antennas, and transmission lines that require a conversion from an unbalanced to a balanced line or vice versa. The performance of the circuits often depends on the performance of the balun. Despite the evolution of the balun, information about the device can be confusing [6]. There are entire books about how to design and construct baluns. This chapter presents general information about baluns, focusing on baluns that are commonly used for electrically small antennas, and on their performance.

2.1 Definition

A balun is a three-port device with a single-ended input and differential output. The term balun is an abbreviation for BALanced-to-UNbalanced. The balun is a passive and reversible device. This means that the differential port can be used as the input and the singled-ended port as an output [9],[15]. A signal splits with the same magnitude and opposite phase when the balun is used to convert from single stage to a differential stage as shown in Figure 2.1 (a). A balun that combines two signals with the same magnitude and opposite phase results in a singled-ended stage, as shown in Figure 2.1(b). Despite the fact that baluns are reversible, it is more common to use them as splitters than as combiners [15]. This thesis analyzes baluns as a devices that can convert a from an unbalanced line (single ended) to a balanced line (differential); in other words, baluns as splitters.

Figure 2.2 presents the characteristics of an ideal balun. They are outlined

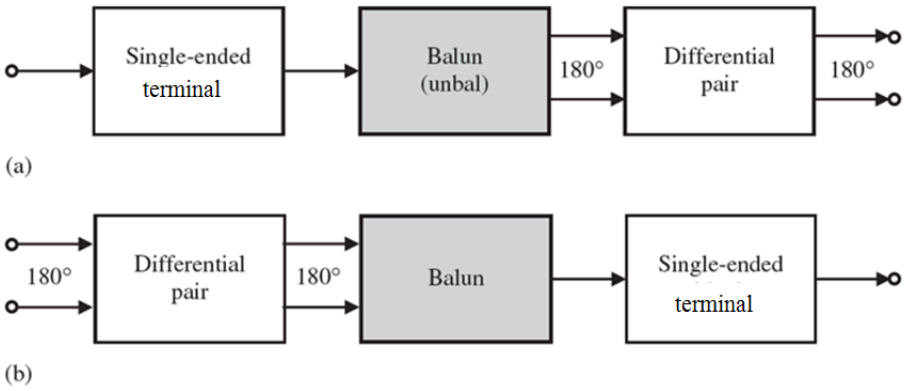

Figure 2.1: A balun, connects single-ended terminal and a differential pair (a) From single-ended terminal to differential pair (b) From differential pair to single-ended terminal. After [15]

as follows [9],[14],[15]:

- Baluns have three terminals: a single-ended terminal and two differential terminals. Usually, the impedance looking into the terminal is 50 Ω at all three terminals. Other impedances can be used, but impedances at the differential terminals must be the same.
- At the differential terminals, the magnitudes of the signals are equal and opposite. In the frequency domain this means the outputs have a 180 ° phase shift.
- Total insertion loss from the single-ended terminal to the differential terminals is zero.
- The power of the signal at each differential terminal is 3 dB lower than that at the single-ended terminal. In practice, it is more than 3 dB lower and the insertion loss is never zero.
- The ideal S-parameters are:

$$S_{12} = -S_{13} = S_{21} = -S_{31}$$

It is often said that a balun is a type of transformer, but it is more precise to say that a transformer can be used as a balun [9]. The reason is because

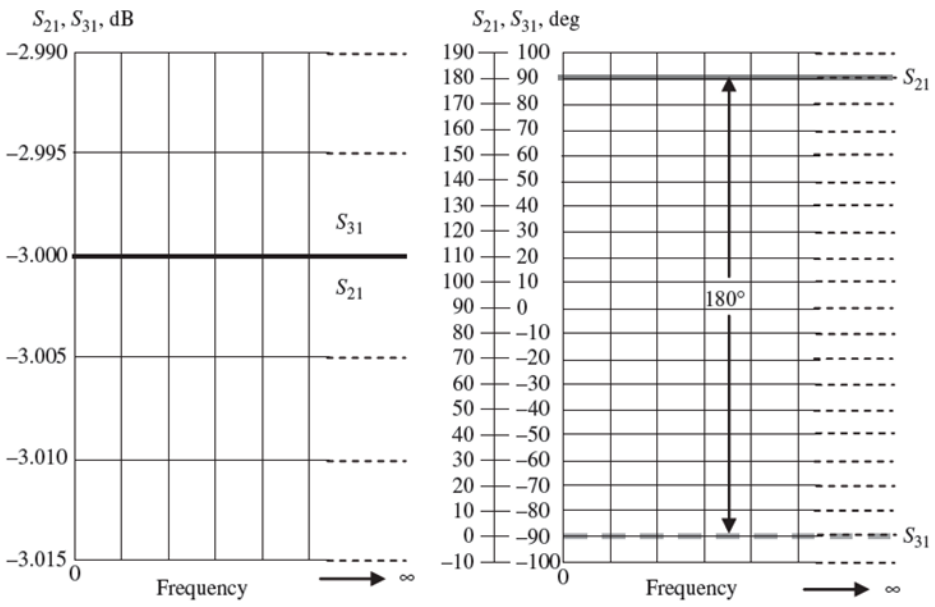

Figure 2.2: Insertion loss and phase shift of an ideal balun [15]

at low frequencies the balun is implemented using a coupled transformer. In RF circuits the most popular baluns are the transformer, LC and microstrip lines. For antenna applications, ferrite bends and cable baluns (sleeve or bazooka) are more commonly used [15]. Cable baluns are never employed in circuitry because of their size. They are useful in laboratory testing where size is not a problem [5].

2.2 Balun in Measurements of Electrically Small Antennas

The 1:1 balun is commonly used in antenna applications. The most popular forms of the 1:1 balun are the bazooka balun, ferrite beads over coaxial line and ferrite-core or air core designs [5]. Ferrite core baluns are often used at lower frequencies due to their compact size and performance. However, they are not recommended in electrically small antenna measurements. It has been shown that a consistent radiation pattern can be difficult to achieve using ferrite chokes because at certain frequencies, depending on dimensions and material properties, ferrite cores can act as lossy resonators. This extra

loss can load the antenna and change its performance [16].

2.2.1 Bazooka (Sleeve) Balun

The quarter-wave bazooka balun, also known as a sleeve balun, is used to measure small antennas at low frequencies (VHF range). The design requires a $\lambda/4$ metal sleeve shorted at its end. The sleeve encapsulates the coaxial line [12]. Input impedance will be very high and common current will be suppressed at the quarter-wavelength frequency [17]. A diagram of a sleeve balun is shown in Figure 2.3, where L is its length, R_1 is the outer conductor of the coax cable, R_1 is the radius of the metal sleeve and T is the thickness of the sleeve. Baluns can be analyzed using transmission line theory. The balun impedance can be represented as a short circuit series stub, $Z_c = Z_0 \tan\beta$, as shown in Figure 2.4 where Z_0 is determined from the ratio of the two radii R_1 and R_2 [12], [17].

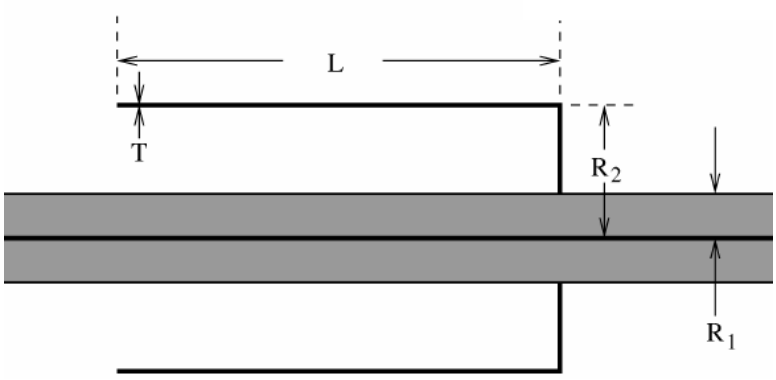

Figure 2.3: Sleeve balun diagram [12]

If measurements are made over a frequency range, the sleeve balun will have high impedance only at one frequency. One way to improve the balun performance over a band is by choosing a high characteristic impedance Z_0, but this is not practical option. In order to maintain the highest possible value of Z_0 for a given outer radius, the thickness of the sleeve must be as small as practicable. Also, the coaxial cable has to be as small as possible, but robust enough to withstand repeated connection and disconnection [12].

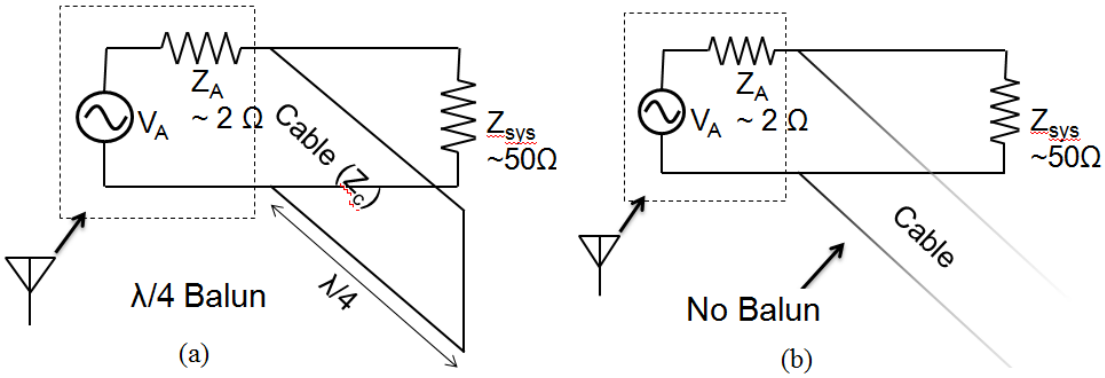

Figure 2.4: Balun T-line model [17]

2.2.2 Folded Bazooka Balun

The folded bazooka balun is very similar to the quarter-wavelength bazooka balun. For the folded design, as the name suggests, the outer sleeve of the balun is folded on itself as shown in Figure 2.5. The advantage of the folded balun over the quarter-wavelength balun is that the length is reduced and another frequency of operation is added [17].

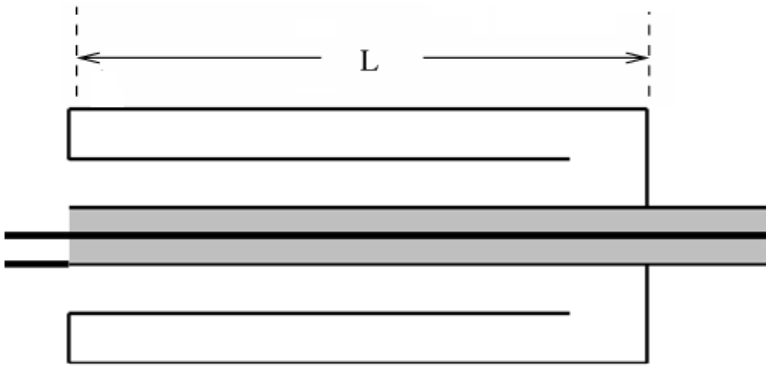

Figure 2.5: Folded bazooka balun diagram [12]

The eighth-wavelength is a version of the folded balun, typically used in the low MHz range to reduce balun size. Figure 2.6 shows these folded chokes implemented with an array of electrically small antennas. This device was built and tested as reported in [1].

It has been shown that for electrically small antennas, the sleeve balun only reduces the common mode current over a 10% bandwidth or less [17].

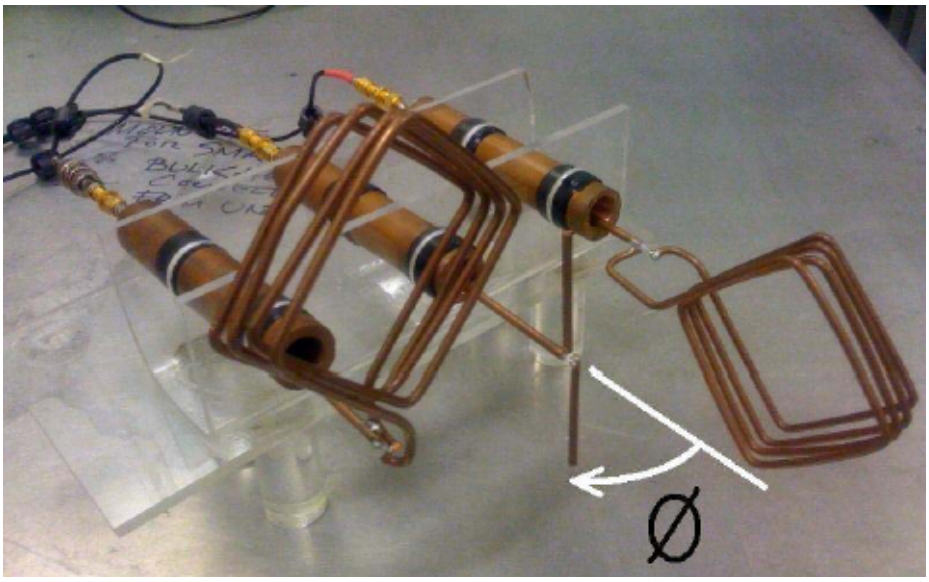

Figure 2.6: Small array of three electrically small antennas, each with its own eighth-wavelength choke designed for operation at 300 MHz [1]

Outside the range of operation, radiation patterns get distorted and repeatable measurements cannot be obtained. Simulations in Ansoft HFSS® of the quarter-wavelength balun and folded balun will be presented in section 2.4. However, to describe the performance of a balun it is first important to understand the concept of common mode rejection ratio. The following section provides a brief summary of common mode rejection ratio in baluns and the mixed-mode S-parameters.

2.3 Common Mode Rejection Ratio

The common mode rejection ratio (CMRR) is used to describe the performance of balanced circuits; it is also known by common mode attenuation, common mode filtering and other names [18]. In a balun, the CMRR is defined as the ratio of wanted to unwanted transmitted power. As rejection of common mode transmission is the primary purpose of a balun, it follows that CMRR is the parameter to determine the performance of the balun [17]. To understand the performance of the balun in suppressing the common mode current, the balun can be modeled as a 1:1 transformer representing the transition between the unbalanced coaxial transmission line and the twin

lead line that feeds the balance antenna [17]. The common mode current I_c is presented with an impedance Z_c, as shown in Figure 2.7

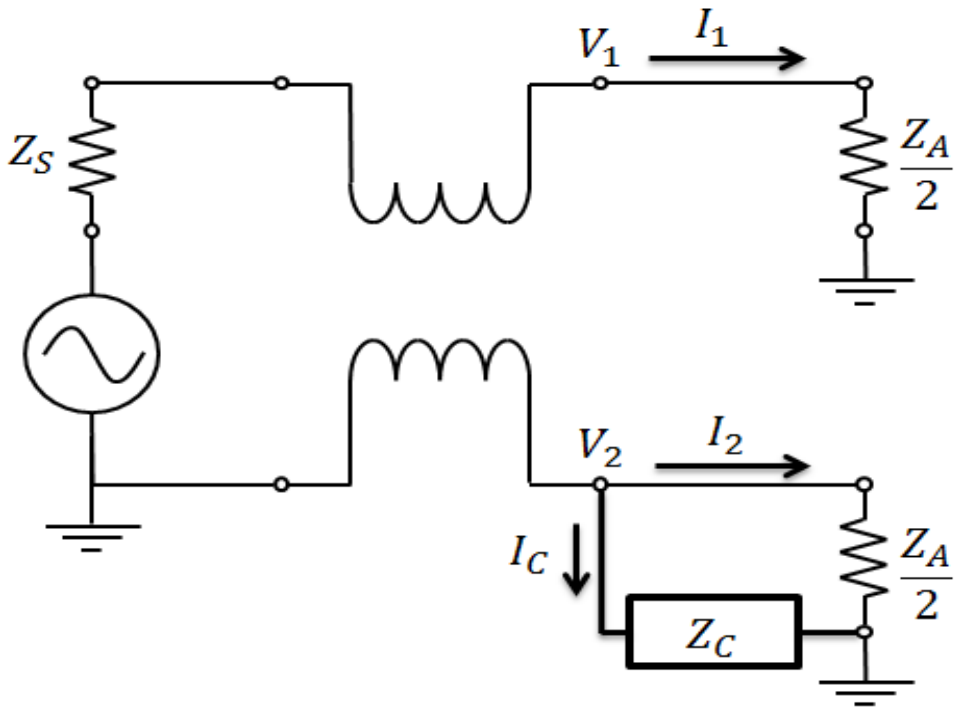

Figure 2.7: Circuit diagram for a common mode choke [17]

The CMRR of a differential fed device, such as the balance port of a balun, is defined as the ratio of the common and differential voltages at the balanced feed.

$$CMRR = \frac{|V_1 + V_2|}{|V_1 - V_2|} \tag{2.1}$$

As the CMRR is defined as the ratio between the differential mode insertion loss and the common mode signal loss, it is given in terms of S-parameters by

$$CMRR = \frac{S_{d1}}{S_{c1}} \tag{2.2}$$

where S_{c1} and S_{d1} are called mixed mode S-parameters between the coaxial cable port of the balun and the common and differential modes of the port. The mixed mode S-parameters can be converted to the single-ended S-parameters. A set of linear equations can be derived that describe the transformation from singled-ended three-port parameters to mixed-mode two-

port. Bockelman and Eisenstadt [19] provide the tools and the math to derive the mixed mode S-parameters to singled-ended S-parameters and vice versa. The following matrix shows the singled-ended S parameters, where [A] is the stimulus and [B] is the response. On the right is a mixed mode representation of the same matrix, where ports 2 and 3 have been combined to form a differential mode port [18],[19].

$$\begin{bmatrix} b_1 \\ b_2 \\ b_3 \end{bmatrix} = \begin{bmatrix} S_{11} & S_{12} & S_{13} \\ S_{21} & S_{22} & S_{23} \\ S_{31} & S_{32} & S_{33} \end{bmatrix} \begin{bmatrix} a_1 \\ a_2 \\ a_3 \end{bmatrix} \Leftrightarrow \begin{bmatrix} b_1 \\ b_d \\ b_c \end{bmatrix} = \begin{bmatrix} S_{11} & S_{1d} & S_{1c} \\ S_{d1} & S_{dd} & S_{dc} \\ S_{c1} & S_{cd} & S_{cc} \end{bmatrix} \begin{bmatrix} a_1 \\ a_d \\ a_c \end{bmatrix}$$

S_{11} in the mixed mode is the same as in the single-ended formulation. The remaining parameters are compound performance parameters. The two most common mixed mode parameters are S_{c1} and S_{d1} with their respective opposites. Parameter S_{d1} is the transmission from port 1 to the mixed mode port, evaluated as a differential port. S_{c1} is the mixed mode transmission parameter from port 1 to the mixed port, evaluated as a common mode port [18],[19].

$$S_{1d} = \frac{1}{\sqrt{2}}(S_{12} - S_{13}) \tag{2.3}$$

$$S_{d1} = \frac{1}{\sqrt{2}}(S_{21} - S_{31}) \tag{2.4}$$

$$S_{1d} = \frac{1}{\sqrt{2}}(S_{12} + S_{13}) \tag{2.5}$$

$$S_{d1} = \frac{1}{\sqrt{2}}(S_{21} + S_{31}) \tag{2.6}$$

The return loss performance of the mixed port is evaluated by S_{dd} and $S_{cc}S_{dd}$ gives the differential return loss, while S_{cc} gives the common mode return loss [18]. The last two parameters S_{cd} and S_{dc} give the transmission parameters from common to differential mode signals [18],[19].

$$S_{dd} = \frac{1}{2}(S_{22} - S_{23} - S_{32} + S_{33}) \tag{2.7}$$

$$S_{dc} = \frac{1}{2}(S_{22} + S_{23} + S_{32} - S_{33}) \tag{2.8}$$

$$S_{cc} = \frac{1}{2}(S_{22} + S_{23} + S_{32} + S_{33}) \tag{2.9}$$

$$S_{cd} = \frac{1}{2}(S_{22} - S_{23} + S_{32} - S_{33}) \tag{2.10}$$

The CMRR is:

$$CMRR = \frac{S_{d1}}{S_{c1}} \Leftrightarrow \frac{\frac{1}{\sqrt{2}}(S_{12} - S_{13})}{\frac{1}{\sqrt{2}}(S_{12} + S_{13})} \Leftrightarrow \frac{S_{12} - S_{13}}{S_{12} + S_{13}} \tag{2.11}$$

The CMRR is dependent on the amplitude and phase of the balun. The relationship between amplitude balance, phase balance, and CMRR is shown in Figure 2.8. A 0.1 dB improvement in amplitude balance will improve the CMRR by the same amount as a 1 deg improvement in phase balance [18]. A good balun can achieve 25-55 dB of CMRR while a low performance balun will have 15-20 dB of CMRR [17].

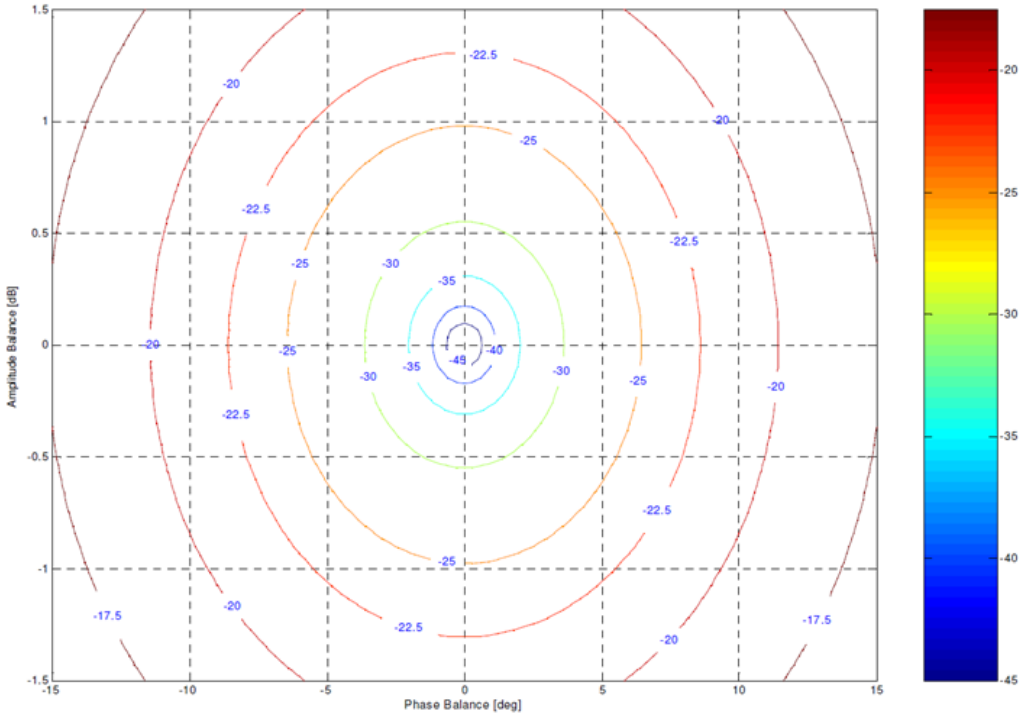

Figure 2.8: Contour plot of CMRR values in [dB] for phase and amplitude [18]

2.4 Performance of Sleeve Balun

In general, sleeve baluns are large compared to the antenna, but they do perform very well. The baluns used in the measurements of this element are effective chokes over a bandwidth of about 15 MHz for CMRR values greater than 45 dB. A CMRR of about 45 dB or higher is desirable [20].

The quarter-wavelength balun of Figure 2.9(a) and the folded balun of Figure 2.9(b) were simulated in Ansys HFSS 14.0. The quarter-wavelength was designed to be operational at a frequency of 350 MHz, with a length $l = \lambda/4 = 214$ mm. The common mode rejection ratio is shown as a function of frequency in Figure 2.10(a). The peak of this graph represents the frequency where the balun performs well, balancing the current on the output port. The quarter-wavelength balun has a peak of 345 MHz, close to the designed frequency. If the balun is simulated or measured at higher frequencies than f_0, it can perform well at f_o, $3f_o$, $5f_o$. The CMRR of the folded balun, shown in Figure 2.10(b), shows that the balun is operational at frequencies of 373 MHz and 740 MHz (l=0.165λ and l=0.31λ). The first two frequencies of operation for this balun are approximately f_o and $2f_o$, where f_o is the lowest frequency of operation.

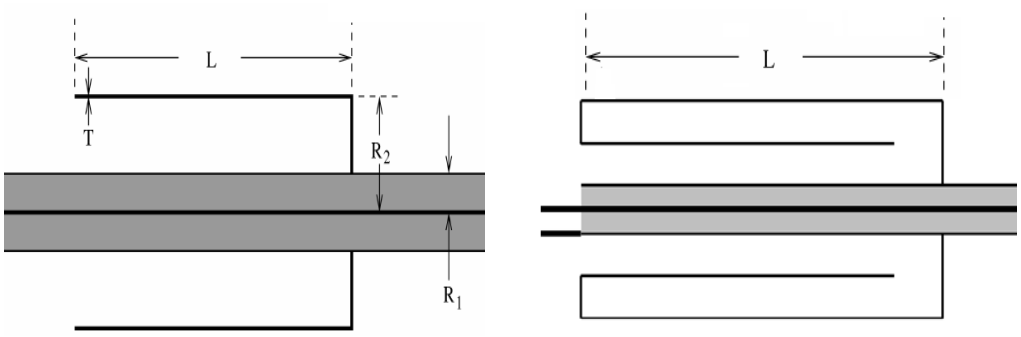

(a) Sleeve Balun Diagram (b) Folded Bazooka Balun Diagram

Figure 2.9: Cross sections of the quarter-wavelength bazooka balun and folded balun simulated in HFSS [12]

An antenna was attached to the quarter-wavelength balun to analyze the radiation pattern of an antenna. Figure 2.11(a) shows the radiation pattern at 350 MHz and 500 MHz. At the frequency of 350 MHz, the radiation pattern is slightly shifted, and at 500 MHz, the radiation pattern is completely distorted. It can be concluded from the simulation results that this type

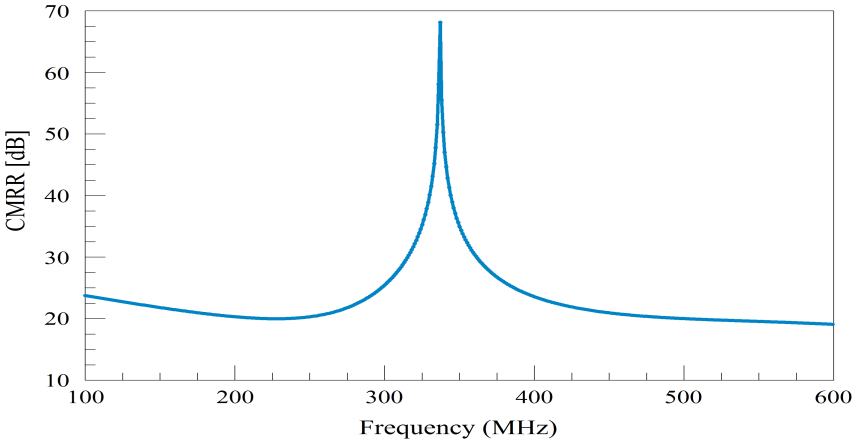

(a) Quarter-wavelength sleeve balun

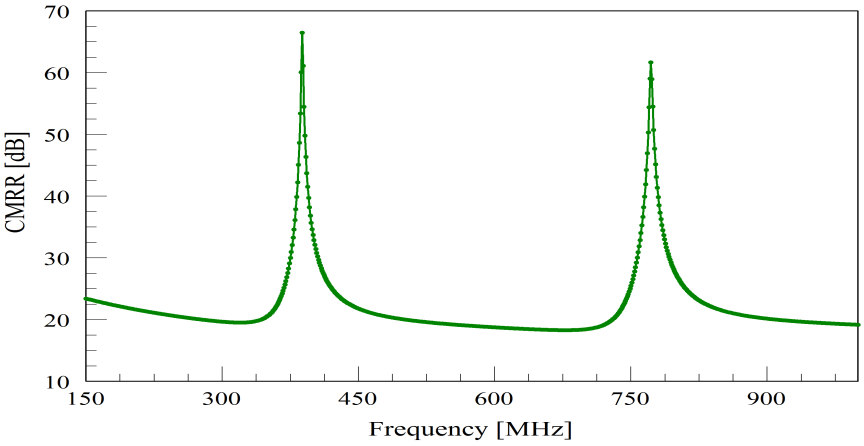

(b) Folded balun

Figure 2.10: CMRR sleeve baluns

of balun distorts the radiation pattern near the frequency of operation. The simulated operation frequency for this balun was 345 MHz. At this frequency, the radiation pattern is accurate.

Slater and Bernhard [20] studied the current distribution on the balun when an electrically small dipole antenna is attached. They found that only at the balun design frequency was the cable current balanced. The result is a uniform distribution on both arms of the dipole and very low common current on the cable as shown in Figure 2.12(b). In contrast, if the device is driven at any frequency other than the operational frequency of the balun, the current on the dipole is unbalanced and the magnitude of the cable current is high, as shown in Figure 2.12(a).

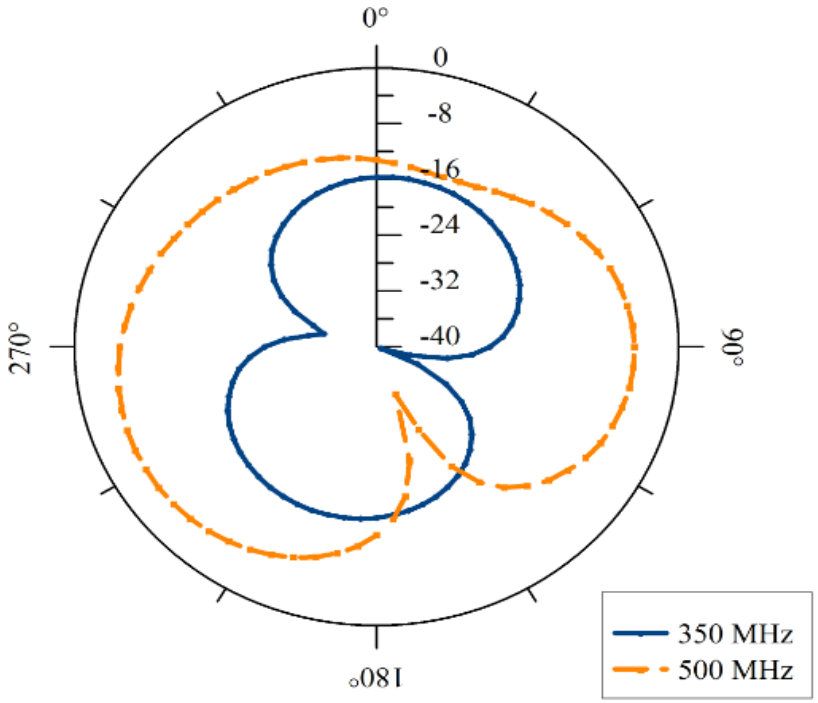

Figure 2.11: Radiation pattern at 350 MHz and 500 MHz

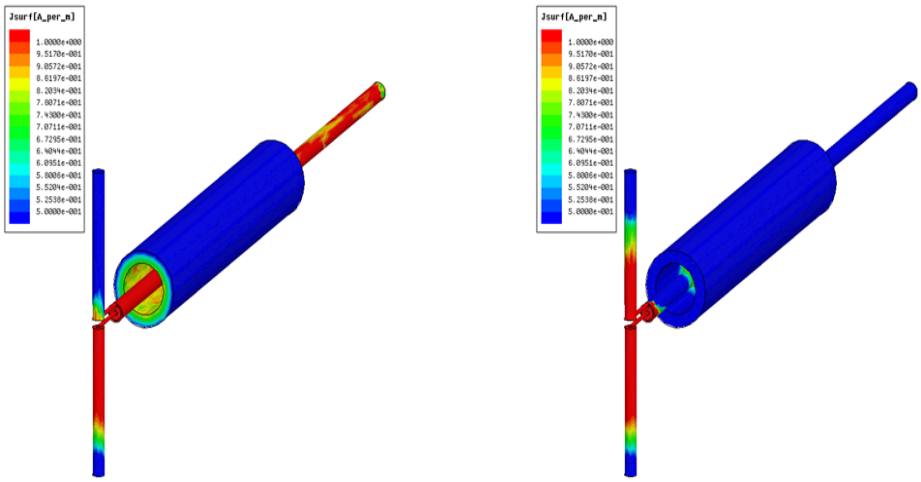

(a) Unbalanced Current (b) Balanced Current

Figure 2.12: Unbalanced/balanced antenna current [20]

CHAPTER 3

BALUN DESIGN AND SIMULATIONS

Designing a wideband balun is a challenge. Different wideband baluns have been published, such as the N-section half-wave balun [21] and the log-periodic balun [22]. However, they are all designed for high frequencies, in the low GHz range (approximately 3 GHz to 6 GHz). This made fabrication easier as the balun size is inversely proportional to the operational frequency. Another motivation to design in the low GHz range is that the frequency band for ultra wideband communication systems is 3.1-10.6 GHz. Therefore, UWB antennas have attracted great attention in recent years as well as the way to feed them properly [23].

On the other hand, wide-band operation baluns for low frequencies (MHz) have been rarely explored. Design and performance characteristics of a sleeve balun structure are proposed in this chapter in order to achieve wide-band operation in the low frequency range. The design is based on the log-periodic antenna theory. Design guidelines and techniques to achieve wide-band are presented in this chapter.

3.1 Development of a Log Periodic Bazooka Balun Structure

The proposed design is based on the quarter-wave bazooka balun consisting of resonators arranged in log-periodic manner where $\tau < 1$ is the period of the structure. The main objective of this design is to have high impedance and therefore high common mode rejection ratios at various different frequencies. To do so, there needs to be a short at the quarter-wavelength corresponding to each of these frequencies. This can be accomplished by inserting resonant series LC circuits. The circuits are placed between the outer shield of the coaxial cable and the inner wall of the balun as shown in Figure 3.1.

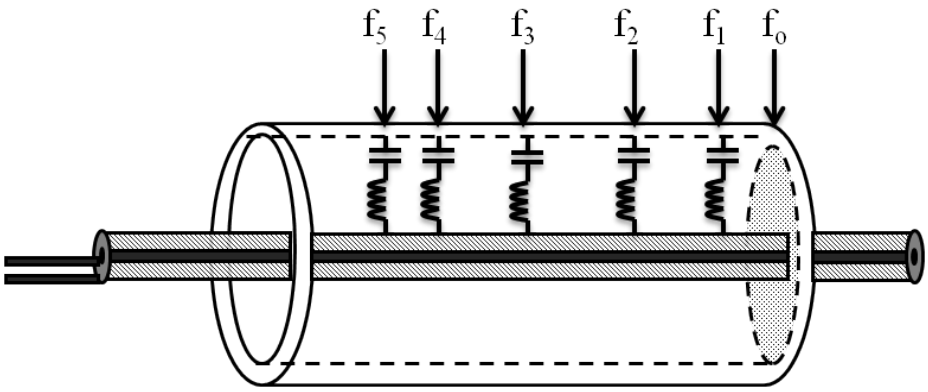

Figure 3.1: Log periodic wideband concept

The spacing of resonators in the balun is governed by:

$$\tau = \frac{d_{n+1}}{d_n} = \frac{\lambda_{n+1}}{\lambda_n} = \frac{f_n}{f_{n+1}} \tag{3.1}$$

where τ is the geometric ratio (< 1), d is the distance between resonators, λ is the wavelength and f is the frequency of operation. By choosing the specific τ value, the resonant frequencies can be calculated as

$$f_0 = \tau f_2 = \tau^2 f_1 = \tau^3 f_2 = \tau^4 f_3 \tag{3.2}$$

$$f_0 < f_1 < f_2 < f_3$$

which implies that

$$\lambda_3 = \tau \lambda_2 = \tau^2 \lambda_1 = \tau^3 \lambda_0 \tag{3.3}$$

$$\lambda_3 < \lambda_2 < \lambda_1 < \lambda_0$$

and

$$d_3 = \tau d_2 = \tau^2 d_1 = \tau^3 d_0 \tag{3.4}$$

$$d_3 < d_2 < d_1 < d_0$$

In order to place the resonators between the outer shield of the coaxial cable and the inner wall of the balun, circular slotted disks need to be implemented as shown in Figure 3.2. These are intended to create short circuit terminations at the different design frequencies.

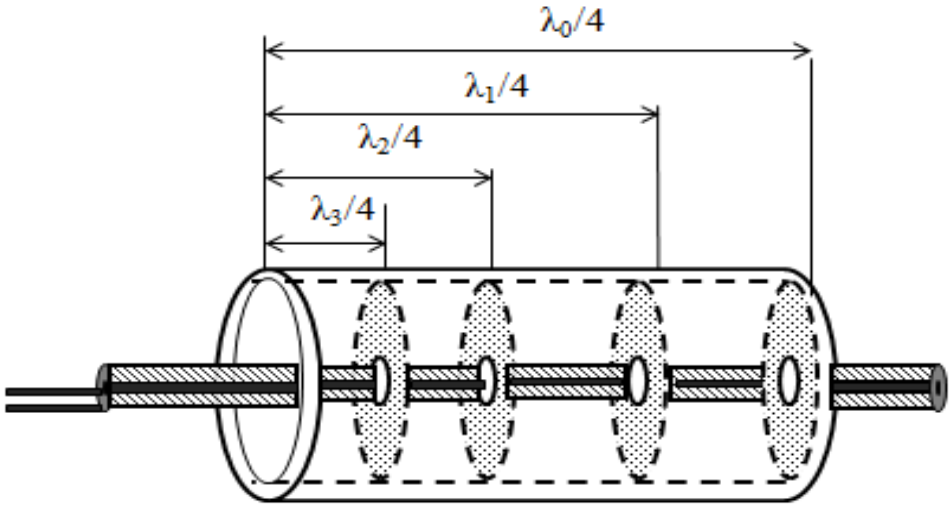

Figure 3.2: Log periodic wideband concept

3.2 Equivalent Circuit Model

According to transmission line theory, the circuit model can be represented as a cascade of sections of the transmission line with characteristic impedance Z_0 and length θ_n with shunt impedance Y_n as shown in Figure 3.3. This shunt impedance consists of LC circuits; however, losses in the inductors need to be taken into account. These losses, represented as R_n, will be introduced in the following sections.

The characteristic impedance Z_0 can be determined as in a coaxial cable, from the ratio of the inner and outer conductor diameter and the dielectric constant ε_r. The outer diameter of the inner conductor is $a = 3.5$ mm, which is the outer conductor of the coaxial cable. The inner diameter of the outer conductor of the balun is $b = 19.55$ mm. This device can achieve high CMRR if the characteristic impedance is high; therefore, the balun's diameter was chosen as high practically as possible. From the equation of coaxial cable [24], the characteristic impedance Z_0 of the balun can be determined as

$$Z_0 = \frac{138\Omega}{\sqrt{\varepsilon_r}} log_{10} \frac{b}{a} \tag{3.5}$$

$$Z_0 = 103\ \Omega$$

where $\varepsilon_r = 1$

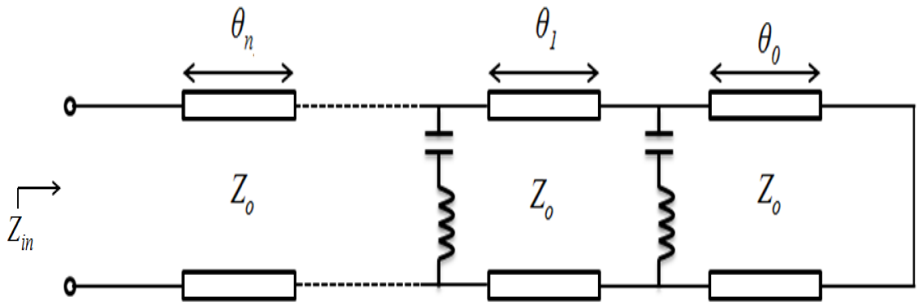

Figure 3.3: Equivalent circuit

The transmission line impedance equation for an arbitrary load is given by

$$Z_{in} = Z_0 \frac{Z_L + jZ_0 \tan \beta l}{Z_0 + jZ_L \tan \beta l} \tag{3.6}$$

If the line is a quarter-wavelength long, the input impedance is given by

$$Z_{in} = \frac{Z_0^2}{Z_L} \tag{3.7}$$

Since the LC circuits are placed to create short-circuit terminations at different design frequencies, we can approximate $Z_L = 0$ at each of the design frequencies. Therefore,

$$Z_{in} \approx \infty$$

3.2.1 High Frequency Characteristics of Passive Components

The ideal equivalent circuit model was shown in Figure 3.3; however in high frequency ranges an equivalent circuit model may be more complex than the low-frequency circuit model. Passive components such as resistors, capacitors, and inductors incur dielectric and/or ohmic loss [25]. This effect needs to be accounted for in the analysis and design of practical circuits. For this design, effects due to the capacitor will be neglected, but effects in the inductor will be considered.

An accurate equivalent circuit for an inductor includes a series resistance to model the ohmic losses and a shunt capacitance to account for the capaci-

tance between the turns of the coil (See Figure 3.4). Two parameters will be considered due to this distributed equivalent circuit: self-resonant frequency (SRF) and the Q factor.

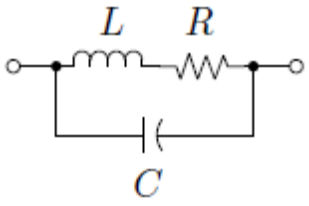

Figure 3.4: Equivalent circuit for an inductor [25]

The SFR parameter is the inductor self-resonant frequency (SRF). It is an important parameter to take into account for RF/microwave applications. Any type of inductor will exhibit some capacitance. Therefore, the inductor will serve as a parallel resonant circuit with a self-resonant frequency. For inductors used in choke applications, the best signal suppression occurs at the SRF where the impedance is at maximum. Below an inductor's SRF, impedance decreases with decreasing frequency [26] as shown in Figure 3.5. Therefore, it is important to make sure that an inductor has a very large impedance near the parallel resonant frequency.

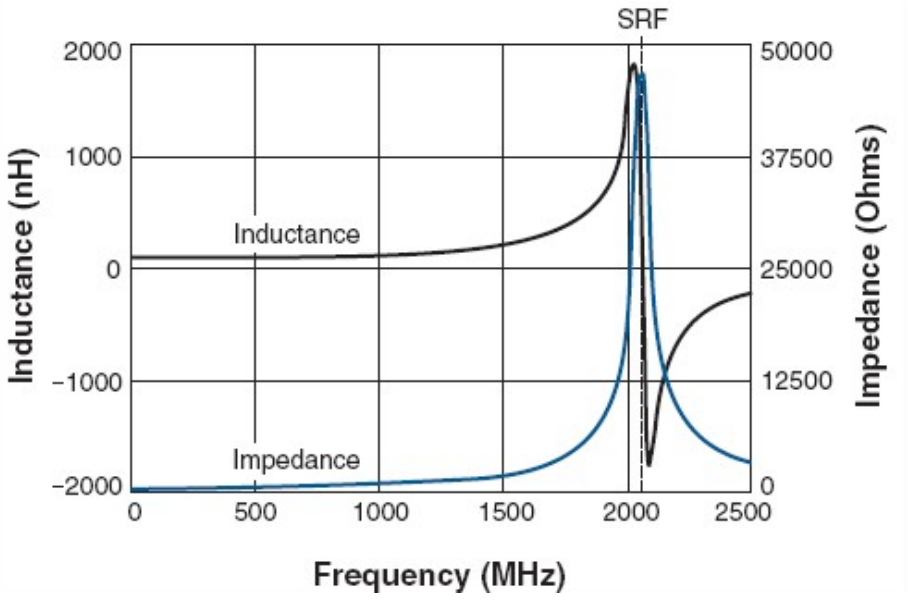

Figure 3.5: An inductance and impedance rise sharply at 2000 MHz [26]

The quality, or Q, factor is a dimensionless parameter that characterizes a circuit's bandwidth relative to its center frequency, with high Q values associated with narrow bandwidth [25],[26]. The Q factor of an inductor can be calculated as a ratio of the inductor's imaginary impedance, $Im[Z]$, to its real impedance, $Re[Z]$

$$Q = \frac{|X_s|}{R_s} \tag{3.8}$$

where the impedance of the inductor is $Z = R_s + jX_s$.

3.2.2 Frequency Response: Resonance, Bandwidth, Q Factor

Each resonant circuit can be analyzed as an individual series RLC circuit [24] as shown in Figure 3.6.

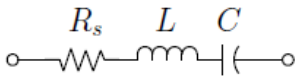

Figure 3.6: Series RLC circuit [25]

The voltage transfer function is

$$H(s) = \frac{R}{R + sL + \frac{1}{sC}} \tag{3.9}$$

If sinusoidal excitation is considered under steady-state conditions, the frequency response $H(j\omega)$ is

$$H(j\omega) = \frac{R}{R + j\omega L(1 - \frac{1}{\omega^2 LC})} \tag{3.10}$$

When $\omega = \frac{1}{\sqrt{LC}}$, the phase shift of the transfer function is zero; this is called the resonant frequency, ω_o, of the network and is the frequency at which the inductive and capacitive reactances are exactly equal in magnitude and, consequently, cancel each other:

$$\omega_o = \frac{1}{\sqrt{LC}} \Rightarrow f_o = \frac{1}{2\pi\sqrt{LC}} \tag{3.11}$$

At resonance

$$\omega_o L = \frac{1}{\omega_o C} \tag{3.12}$$

Also, the quality factor Q_s for the series RLC circuit is defined as the relationship between the inductance for the resonant frequency and the resistance.

$$Q_s = \frac{\omega_o L}{R} = \frac{1}{\omega_o C R} = \frac{1}{R}\sqrt{\frac{L}{C}} \tag{3.13}$$

The parameter Q_s is referred to as the series resonant circuit Q. The inverse of this quantity tells what fraction of the total energy stored in the RLC circuit is dissipated in one complete cycle of the resonant frequency. The frequency response function can be rewritten in terms of ω_o and Q_s:

$$H(j\omega) = \frac{1}{1 + jQ_s(\frac{\omega}{\omega_o} - \frac{\omega_o}{\omega})} \tag{3.14}$$

The magnitude of the voltage transfer function as a function of normalized frequency is shown in Figure 3.7. The circuit behaves as a band-pass filter allowing signal components close to the resonance frequency, while rejecting (partially) the higher and lower frequency components.

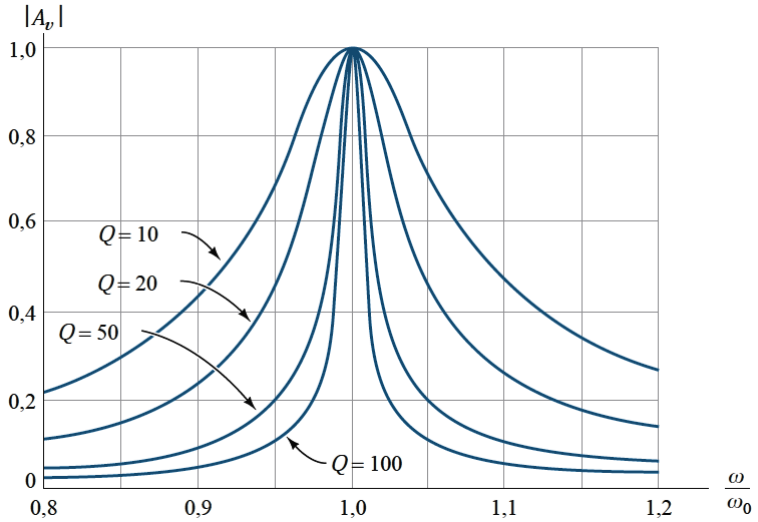

Figure 3.7: Magnitude of the voltage transfer function [26]

The bandwidth of a series RLC filter is inversely proportional to the Q_s of the circuit.

$$BW = \Delta\omega = (\omega_H - \omega_L) \tag{3.15}$$

$$BW = \frac{\omega_o}{Q_s} \tag{3.16}$$

where the cut off frequencies are:

$$\omega_H = \omega_o - BW/2 \tag{3.17}$$

$$\omega_L = \omega_o + BW/2 \tag{3.18}$$

3.2.3 ABCD Parameters

The equivalent circuit of the wideband balun is a cascade of transmission line sections with shunt impedance sections (see Figure 3.8). The best way to analyze this network is to use an ABCD matrix, a set of network parameters particularly suited for cascading two-port networks. The usefulness of the ABCD matrix is that cascaded two-port networks can be characterized by simply multiplying their ABCD matrices [24]. The elements of the ABCD matrix may be converted to the elements of the Z matrix, Y matrix, and S matrix and vice versa by using mathematical formulations. The following ABCD matrix represents the equivalent circuit model for two resonators and three sections of transmission line. This result can be extended for the case of any number of networks in cascade:

$$\begin{bmatrix} A_x & B_x \\ C_x & D_x \end{bmatrix} = \begin{bmatrix} A_0 & B_0 \\ C_0 & D_0 \end{bmatrix} \begin{bmatrix} A_1 & B_1 \\ C_1 & D_1 \end{bmatrix} \begin{bmatrix} A_2 & B_2 \\ C_2 & D_2 \end{bmatrix} \begin{bmatrix} A_3 & B_3 \\ C_3 & D_3 \end{bmatrix} \begin{bmatrix} A_4 & B_4 \\ C_4 & D_4 \end{bmatrix} \tag{3.19}$$

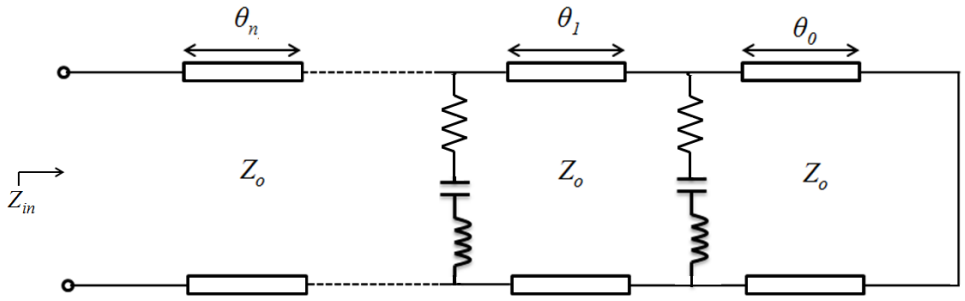

Figure 3.8: Equivalent circuit for analysis and simulations

where

$$\begin{bmatrix} A_0 & B_0 \\ C_0 & D_0 \end{bmatrix} = \begin{bmatrix} \cos(\beta l_0) & jZ_0 \sin(\beta l_0) \\ jY_0 \sin(\beta l_0) & \cos(\beta l_0) \end{bmatrix}$$

$$\begin{bmatrix} A_1 & B_1 \\ C_1 & D_1 \end{bmatrix} = \begin{bmatrix} 0 & 1 \\ Y_1 & 0 \end{bmatrix} = \begin{bmatrix} 0 & 1 \\ \frac{\omega C_1}{j\omega^2 L_1 C_1 + \omega R_1 C_1 - j} & 0 \end{bmatrix}$$

$$\begin{bmatrix} A_2 & B_2 \\ C_2 & D_2 \end{bmatrix} = \begin{bmatrix} \cos(\beta l_1) & jZ_0 \sin(\beta l_1) \\ jY_0 \sin(\beta l_1) & \cos(\beta l_1) \end{bmatrix}$$

$$\begin{bmatrix} A_3 & B_3 \\ C_3 & D_3 \end{bmatrix} = \begin{bmatrix} 0 & 1 \\ Y_2 & 0 \end{bmatrix} = \begin{bmatrix} 0 & 1 \\ \frac{\omega C_2}{j\omega^2 L_2 C_2 + \omega R_2 C_2 - j} & 0 \end{bmatrix}$$

$$\begin{bmatrix} A_4 & B_4 \\ C_4 & D_4 \end{bmatrix} = \begin{bmatrix} \cos(\beta l_2) & jZ_0 \sin(\beta l_2) \\ jY_0 \sin(\beta l_2) & \cos(\beta l_2) \end{bmatrix}$$

One parameter that is important is the input impedance of the network. Since the main objective is to achieve high input impedance, Z_{in} is a good parameter to determine the impedance level for the overall circuit. It can be derived from the ABCD parameters as:

$$Z_{in} = \frac{V_1}{I_1} = \frac{A_x Z_L + B_x}{C_x Z_L + D_x} \tag{3.20}$$

3.3 Two-Resonator Design

3.3.1 Choosing the Period and Resonant Frequencies

The frequency range in which the balun satisfies the design requirements will be referred to as the bandwidth of the balun. The first step is to choose an appropriate value of τ in order to determine the resonant frequencies, and therefore the bandwidth. When the value of τ is high, the gaps between resonant frequencies are smaller, but bandwidth becomes narrow. In the design, we started with a balun of length 214 mm, designed at a frequency of 350 MHz. This will be the lowest frequency of operation of the balun. Each subsequent frequency can be determined using Equation 3.1; however, we want the highest frequency to have a value of 750 MHz.

$$f_1 = 350 \text{ MHz} \; ; \; f_3 = 750 \text{ MHz}$$

$$f_1 = \tau^2 f_3$$

$$\tau = \left(\frac{350}{750}\right)^{\frac{1}{2}}$$

$$\tau = 0.683$$

$$f_2 = \frac{f_1}{\tau} = 512 \text{ MHz}$$

$$f_1 = 350 \text{ MHz}; \; f_2 = 512 \text{ MHz} \; ; \; f_3 = 750 \text{ MHz}$$

Wavelength can be calculated using

$$\lambda = \frac{c}{f}$$

$$f_1 = 350 \text{ MHz} \Rightarrow \lambda_1 = 0.857 \text{ m}$$

$$f_2 = 512 \text{ MHz} \Rightarrow \lambda_2 = 0.585 \text{ m}$$

$$f_3 = 750 \text{ MHz} \Rightarrow \lambda_3 = 0.4 \text{ m}$$

where f_1 corresponds to the short in the balun.

Circuit placement is determined by the resonant quarter wavelength at each frequency. Therefore,

$$f_1 = 350 \text{ MHz} \Rightarrow \lambda_1/4 = 214 \text{ mm} \Rightarrow \text{Short}$$

$$f_2 = 512 \text{ MHz} \Rightarrow \lambda_2/4 = 147 \text{ mm} \Rightarrow 2^{nd} \text{ resonator}$$

$$f_3 = 750 \text{ MHz} \Rightarrow \lambda_3/4 = 100 \text{ mm} \Rightarrow 1^{st} \text{ resonator}$$

Figure 3.9 shows the LC circuit placement.

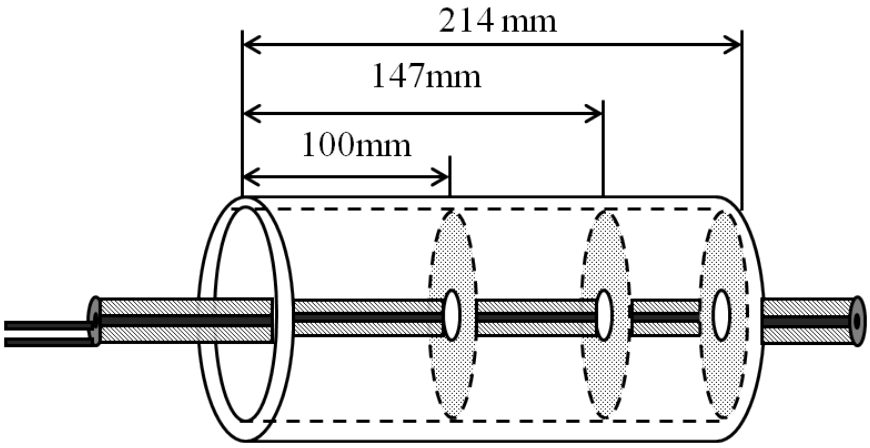

Figure 3.9: Diagram design with two resonators

3.3.2 LC Values and the Q Effect

The inductors are the key circuit element in this design. This component will determine the Q factor of each resonator and therefore the losses in the system. As mentioned previously, high Q values are associated with narrow bandwidth. To study the effect of the quality factor of each resonator, different designs were simulated. It is known that the quality factor is inversely proportional to the bandwidth of the circuit; however, since we are designing two resonators at different frequencies, it was decided to keep the bandwidth of each resonator the same. This will lead to a different Q value for each resonator. It is desirable to have a flat response (CMRR) with values greater than 30 dB over the designed frequency range (350-750 MHz).

Six designs were simulated using ADS® and HFSS® in order to analyze their performance. The simulated structure is presented in Figure 3.10. It is important to note how the elements were arranged. The total impedance

was divided in four sections parallel to each other. This was done due to the circular shape of the balun. A uniform impedance was desired over the area. Each rectangle represents the RLC elements.

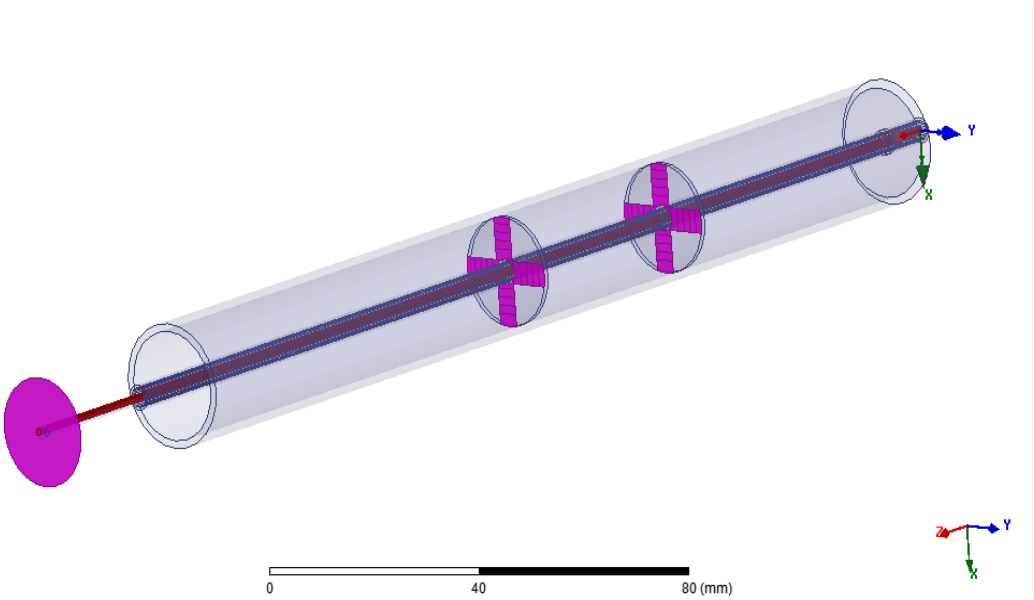

Figure 3.10: Simulated balun using HFSS

The following steps provides a summary of the design:

1. A bandwidth for each resonator was determined.
2. The value of the Q factor was calculated.
3. A practical inductor was found with the desired Q value.
4. Resistance was determined (also provide in inductor's data sheet).
5. Capacitance was calculated.

Tables 3.1, 3.2, 3.3, 3.4, 3.5 and 3.6 provide all the parameters for the different designs. It was chosen to keep the bandwidth constant at values of 5 MHz, 10 MHz, 30 MHz, 50 MHz, 100 MHz and greater than 150 MHz. This bandwidth is the bandwidth of each resonator and not the operational bandwidth of the balun.

Table 3.1: Bandwidth = 5 MHz

f_o **[MHz]**	**L [nH]**	**C [pF]**	**R** [Ω]	**Q factor**
512	30.97	3.14	1.21	102.5
750	29.15	1.54	0.91	150

Table 3.2: Bandwidth = 10 MHz

f_o **[MHz]**	**L [nH]**	**C [pF]**	**R** [Ω]	**Q factor**
512	57.26	1.68	3.75	51.2
750	68.17	0.660	4	75

Table 3.3: Bandwidth = 30 MHz

f_o **[MHz]**	**L [nH]**	**C [pF]**	**R** [Ω]	**Q factor**
512	7.42	13.02	0.94	17.06
750	9.12	4.93	1.41	25

Table 3.4: Bandwidth = 50 MHz

f_o **[MHz]**	**L [nH]**	**C [pF]**	**R** [Ω]	**Q factor**
512	30	3.22	9.42	10.24
750	30	1.5	9.42	15

Table 3.5: Bandwidth = 100 MHz

f_o **[MHz]**	**L [nH]**	**C [pF]**	**R** [Ω]	**Q factor**
512	42.9	2.25	53.45	5.12
750	34.6	1.3	93.8	7.5

Table 3.6: Bandwidth > 150 MHz

f_o **[MHz]**	**L [nH]**	**C [pF]**	**R** [Ω]	**Q**	**BW[MHz]**
512	15.86	6.09	17.0	3	170.6
750	15.86	2.83	25.0	3	250

3.3.3 Simulation Results

HFSS® gives the common mixed-mode S parameters directly using a differential pair at Port 2. Therefore, the CMRR can be calculated using Equation 2.2. Figure 3.11 shows the results obtained.

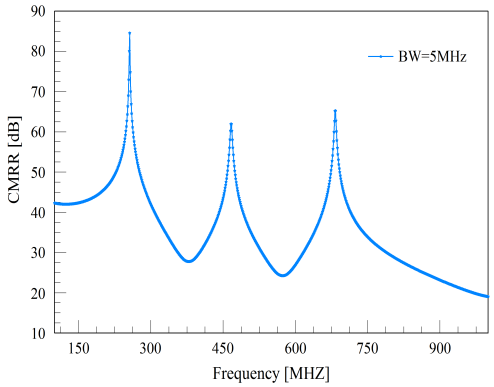

(a) CMRR BW=5 MHz

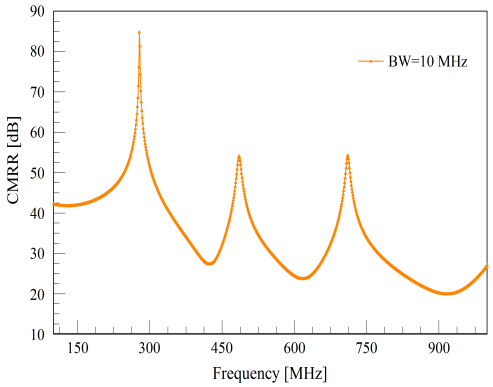

(b) CMRR BW=10 MHz

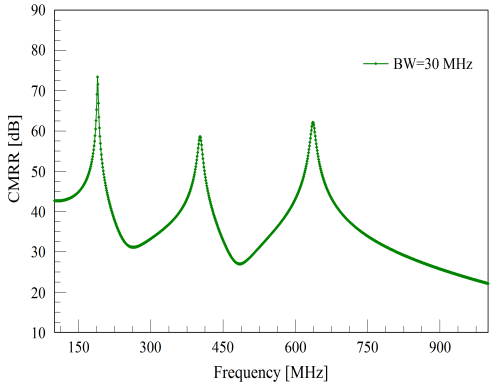

(c) CMRR BW=30 MHz

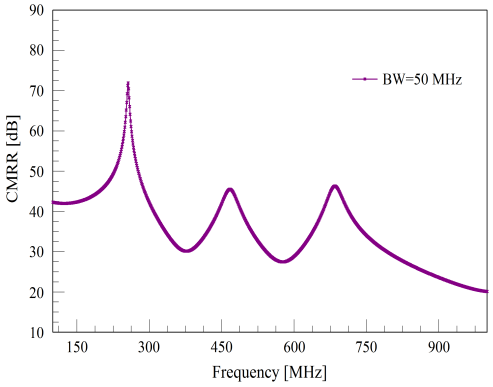

(d) CMRR BW=50MHz

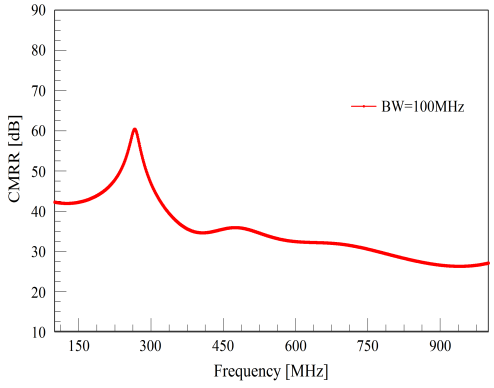

(e) CMRR BW=100 MHz

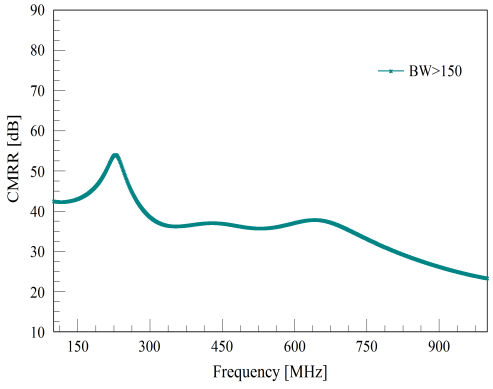

(f) CMRR BW> 150MHz

Figure 3.11: Simulated CMRR two-resonator design

Simulation results in Figure 3.11 show that it is evident that the parameter Q (and therefore the bandwidth) of each resonator affects the response over the range of frequencies. In Figure 3.11(a), 3.11(b) and 3.11(c) where bandwidth is narrow, the peaks are very distinctive in three different frequencies with CMRR values above 50 dB. However, frequencies in between have lower values, below 40 dB. In addition, the peaks of the frequencies are not the frequencies for which the resonators were designed. The response is shifted to lower frequencies. This effect can be observed in all the plots.

In the plots of Figure 3.11(d), 3.11(e) and 3.11(f), the response is smoother over the range of frequencies. This is true especially in plots 3.11(e) and 3.11(f) where the bandwidth of each resonator is greater. These effects are consistent with the theory. As the bandwidth increases, Q decreases and the losses in the system also increase. As a result, the response is flat but CMRR values are lower. The first peak (lower frequency) is due to the short in the structure and not to the resonators. This peak is more difficult to manipulate than the other two frequencies. The responses of 3.11(a), 3.11(c) and 3.11(e) are plotted in Figure 3.12 in order to show in detail the effects described.

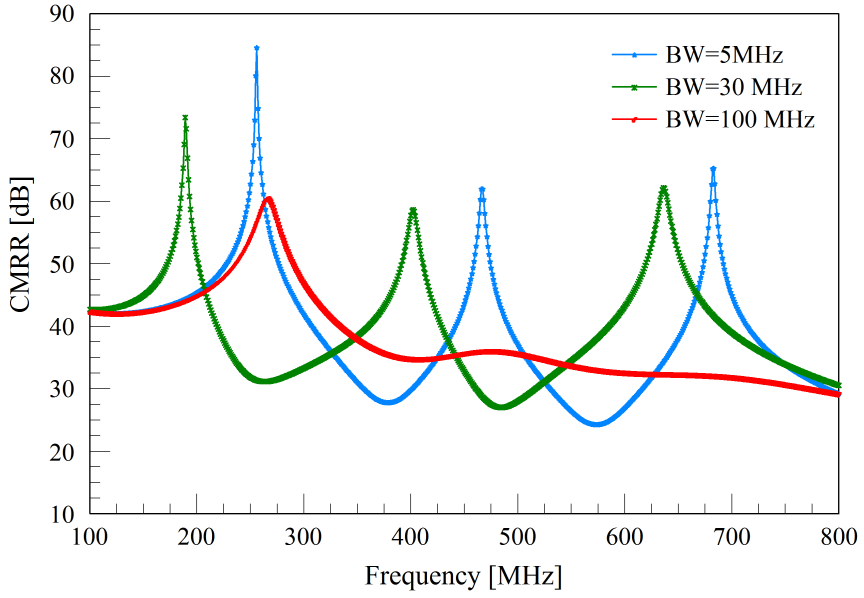

Figure 3.12: Comparison of three different designs with different bandwidths

3.4 Four-Resonator Design

After the analysis of the design of the two resonators, it was decided to introduce two more resonators. The purpose of this new design is to investigate the CMRR increases at values below 30 dB. The range of frequencies is the same as before. Using the same procedure as the previous design, we have frequencies:

$$f_1 = 350 \text{ MHz} \; ; \; f_5 = 750 \text{ MHz}$$

$$f_1 = \tau^4 f_5$$

$$\tau = \left(\frac{350}{750}\right)^{\frac{1}{4}}$$

$$\tau = 0.0.826$$

$$f_2 = \frac{f_1}{\tau} = 423 \text{ MHz}$$

$$f_3 = \frac{f_2}{\tau} = 512 \text{ MHz}$$

$$f_4 = \frac{f_3}{\tau} = 620 \text{ MHz}$$

$$f_1 = 350 \text{ MHz}; \; f_2 = 423 \text{ MHz} \; ; \; f_3 = 512 \text{ MHz};$$

$$f_4 = 620 \text{ MHz}; \; f_5 = 750 \text{ MHz}$$

and wavelengths:

$$f_1 = 350 \text{ MHz} \Rightarrow \lambda_1 = 0.857 \text{ m}$$

$$f_2 = 423 \text{ MHz} \Rightarrow \lambda_2 = 0.7083 \text{ m}$$

$$f_3 = 512 \text{ MHz} \Rightarrow \lambda_3 = 0.5854 \text{ m}$$

$$f_4 = 620 \text{ MHz} \Rightarrow \lambda_4 = 0.4838 \text{ m}$$

$$f_5 = 750 \text{ MHz} \Rightarrow \lambda_5 = 0.4 \text{ m}$$

where f_1 corresponds to the short in the balun.

Circuit placement is determined by the resonant quarter-wavelength at each frequency. Therefore,

$$f_1 = 350 \text{ MHz} \Rightarrow \lambda_1/4 = 214 \text{ mm} \Rightarrow \text{Short}$$

$$f_2 = 423 \text{ MHz} \Rightarrow \lambda_1/4 = 177 \text{ mm} \Rightarrow 4^{th} \text{ resonator}$$

$$f_3 = 512 \text{ MHz} \Rightarrow \lambda_3/4 = 147 \text{ mm} \Rightarrow 3^{rd} \text{ resonator}$$

$$f_4 = 620 \text{ MHz} \Rightarrow \lambda_4/4 = 120.9 \text{ mm} \Rightarrow 2^{nd} \text{ resonator}$$

$$f_5 = 750 \text{ MHz} \Rightarrow \lambda_5/4 = 100 \text{ mm} \Rightarrow 1^{st} \text{ resonator}$$

Figure 3.13 shows the LC circuit placement.

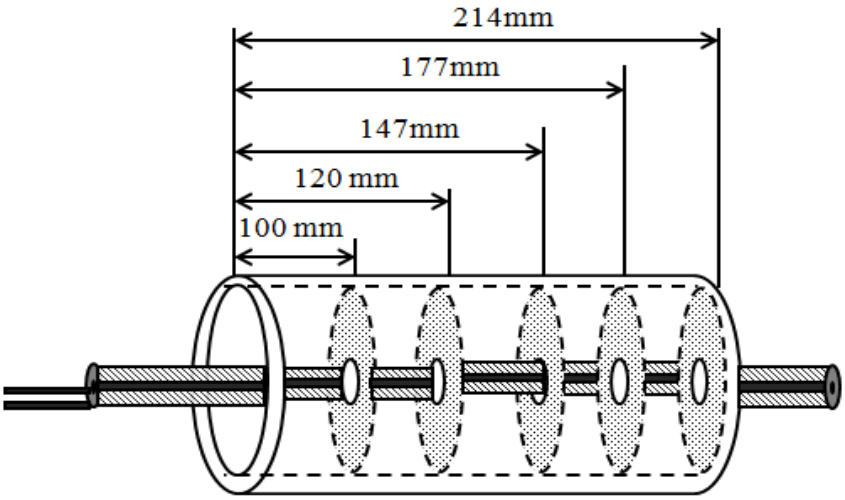

Figure 3.13: Diagram design with four resonators

3.4.1 Choosing LC Values

The same analysis as that for the two-resonator design was performed. The bandwidth was kept constant while the Q value was determined using the operational frequency f_0. The simulated balun is presented in the Figure 3.14. Table 3.7, 3.8, 3.9, 3.10, 3.11 and 3.12 provide all the parameters for the different designs. The circuit elements for the frequencies f_0=512 MHz and $f_0 = 750$ MHz were the same as for the previous design. New components were added for $f_0 = 423$ MHz and $f_0 = 620$ MHz.

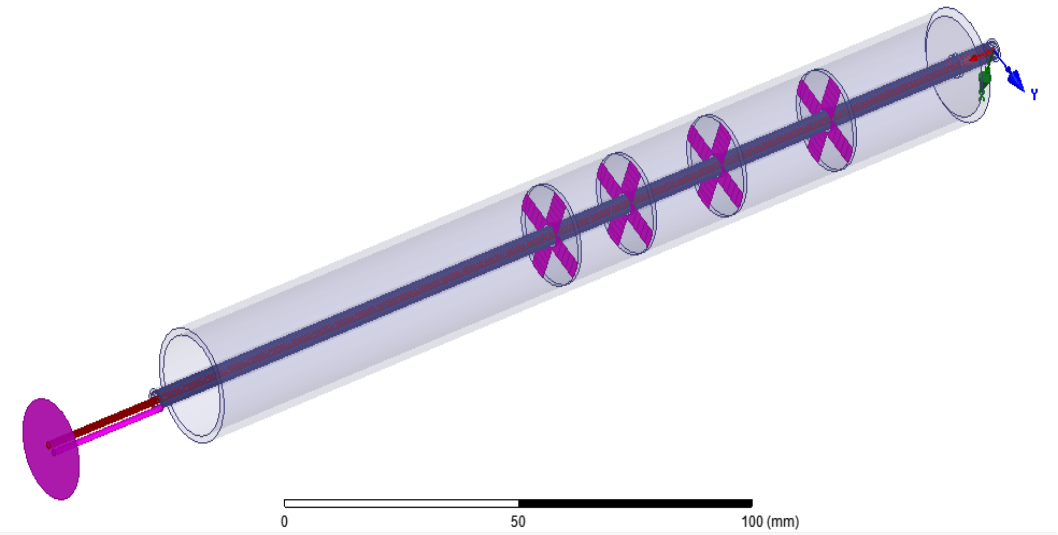

Figure 3.14: Simulated balun using HFSS four LC circuits

Table 3.7: Bandwidth = 5 MHz

f_o **[MHz]**	**L [nH]**	**C [pF]**	**R** [Ω]	**Q factor**
423	37.10	3.8	1.16	85
512	30.97	3.14	1.21	103
620	13.25	5.0	0.41	124
750	29.15	1.54	0.91	150

Table 3.8: Bandwidth = 10 MHz

f_o **[MHz]**	**L [nH]**	**C [pF]**	**R** [Ω]	**Q factor**
423	57.01	2.48	3.58	42
512	57.26	1.68	3.75	51.2
620	70.0	0.94	4.4	62
750	68.17	0.660	4	75

Table 3.9: Bandwidth = 30 MHz

f_o **[MHz]**	**L [nH]**	**C [pF]**	**R** [Ω]	**Q factor**
423	33.34	4.24	6.28	14
512	7.42	13.02	0.94	17.06
620	10.30	6.24	1.94	20.6
750	9.12	4.93	1.41	25

Table 3.10: Bandwidth = 50 MHz

f_o **[MHz]**	**L [nH]**	**C [pF]**	**R** [Ω]	**Q factor**
423	28.82	4.9	9.05	8.46
512	30	3.22	9.42	10.24
620	51.74	1.27	16.25	12.4
750	30	1.5	9.42	15

Table 3.11: Bandwidth = 100 MHz

f_o **[MHz]**	**L [nH]**	**C [pF]**	**R** [Ω]	**Q factor**
423	70.78	2	44.47	4.23
512	42.9	2.25	53.45	5.12
620	32.95	2	20.70	6.20
750	34.6	1.3	93.8	7.5

Table 3.12: Bandwidth > 150 MHz

f_o **[MHz]**	**L [nH]**	**C [pF]**	**R** [Ω]	**Q**	**BW[MHz]**
423	26.83	5.27	23.67	3	141
512	15.86	6.09	17.0	3	170.6
620	24.43	2.70	45	2	310
750	15.86	2.83	25.0	3	250

3.4.2 Simulation Results

The common mode rejection ratio was calculated using Equation 2.2. Figure 3.15 shows the simulated results.

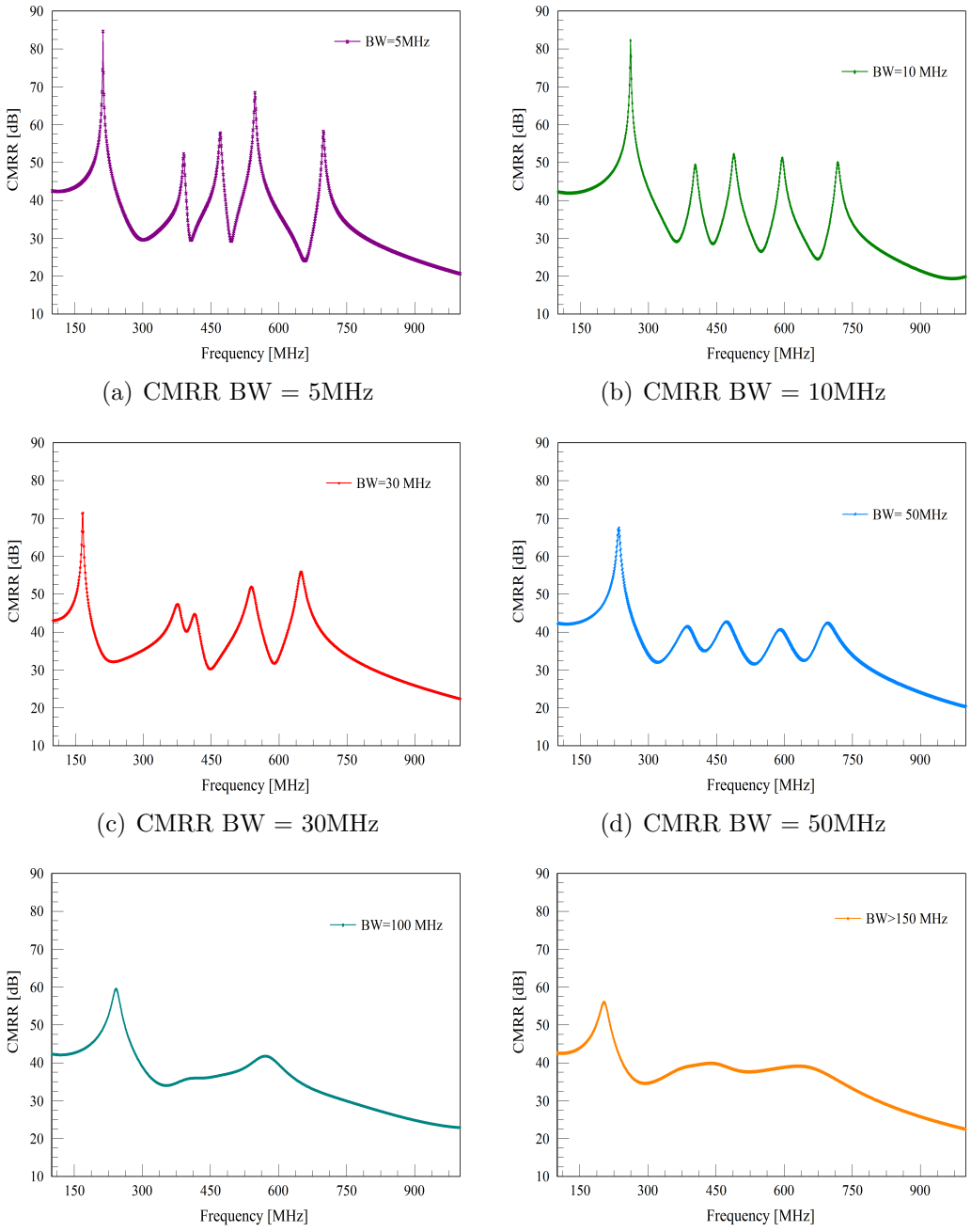

(a) CMRR BW = 5MHz

(b) CMRR BW = 10MHz

(c) CMRR BW = 30MHz

(d) CMRR BW = 50MHz

(e) CMRR BW = 100MHz

(f) CMRR BW > 150MHz

Figure 3.15: Simulated CMRR four-resonator design

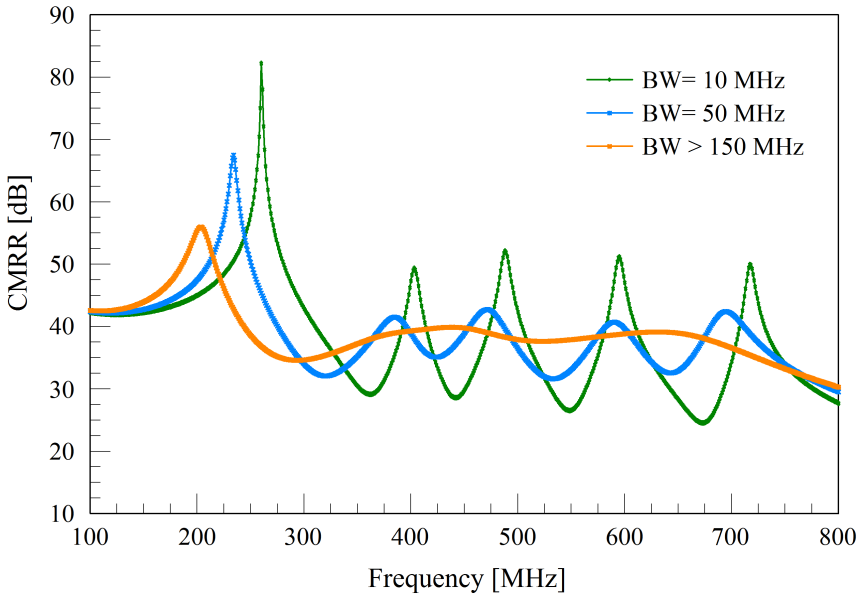

Figure 3.16: Simulated results comparison

A plot is shown in Figure 3.16 to compare the simulated results for wide and narrow bandwidth. The addition of two more LC circuits resulted in two more peaks for designs with high Q values. In contrast, for low Q values the response is flat and very similar to the two-resonator design. Figure 3.17 is a direct comparison of both designs. The average CMRR is indeed higher for four resonators. Despite the fact that that narrow bandwidth has very high CMRR, the response is not smooth. The wider bandwidth design has a smoother response. The CMMR is lower, but a well performing balun is considered to have a CMRR above 30 dB [18].

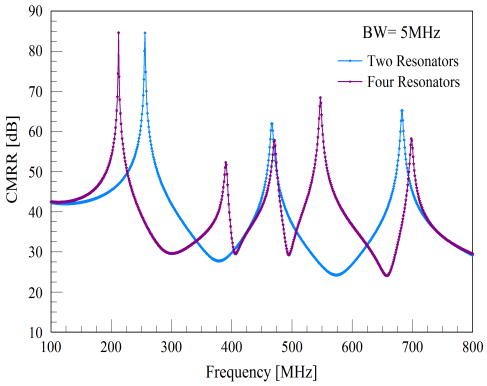

(a) Comparison BW = 5MHz

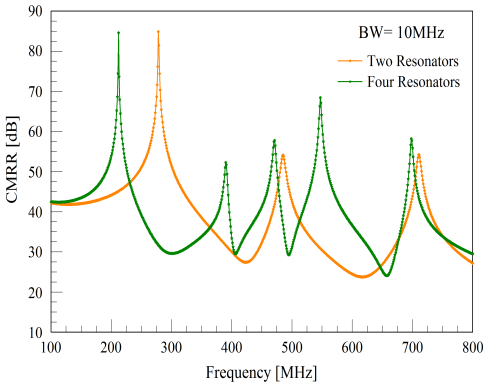

(b) Comparison BW = 10MHz

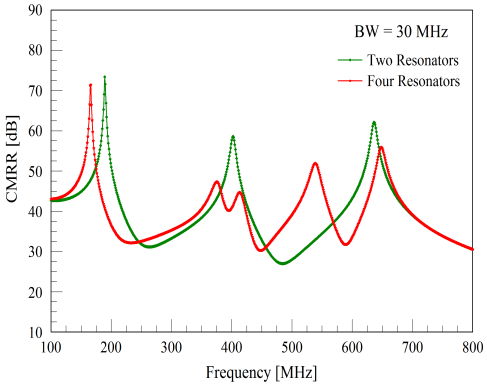

(c) Comparison BW = 30MHz

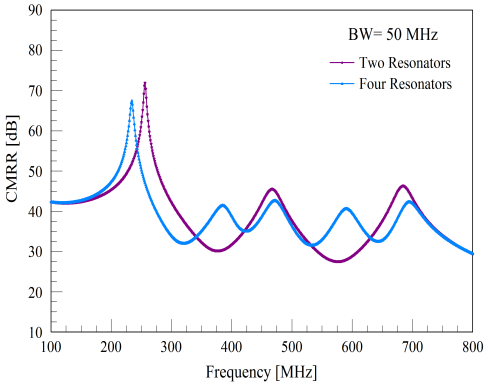

(d) Comparison BW = 50MHz

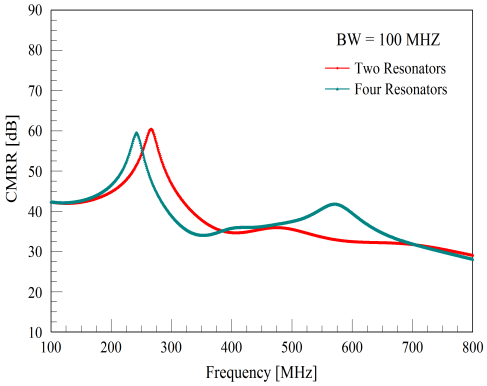

(e) Comparison BW = 100MHz

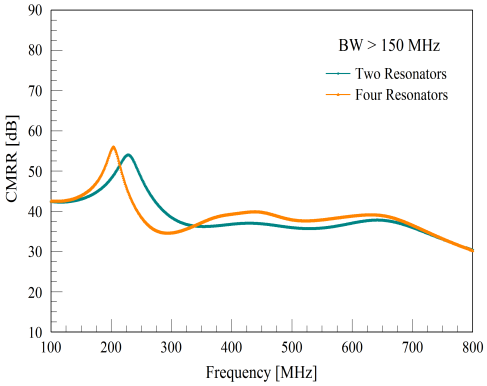

(f) Comparison BW > 150MHz

Figure 3.17: CMRR comparison two and four LC circuits

CHAPTER 4

BALUN CONSTRUCTION AND MEASUREMENTS

Three baluns were built and measured in order to validate and compare with simulations. The first balun was a quarter-wavelength operating at 350 MHz. A second and a third balun were designed with two and four resonators, respectively. Due to the component inventory in the laboratory, it was decided to choose inductors with Q values around 50 and 60 with a bandwidth approximately equal to 10 MHz. Another reason to choose high Q values and narrow bandwidth was that imperfections in the fabrication process introduce losses in the system. The main goal was to achieve a flat response with CMRR greater than 30 dB. In this chapter, the differential probe method, which is the technique that was used here to measure the CMRR of the balun, will be explained. Subsequently, balun construction and results will be presented.

4.1 The Differential Probe Method

To measure the CMRR of the balun chokes, the differential probe method [3] is employed. Because the CMRR is the ratio of the common and differential voltage gains as explain in Chapter 2, by definition it is given in terms of S-parameters as

$$CMRR = \frac{|S_{d1}|}{|S_{c1}|} \tag{4.1}$$

The mixed S-parameters are given in terms of the single-ended S parameters

$$S_{c1} = \frac{1}{\sqrt{2}}\left(S_{21} + S_{31}\right) \tag{4.2}$$

$$S_{d1} = \frac{1}{\sqrt{2}}\left(S_{21} - S_{31}\right) \tag{4.3}$$

To measure these S-parameters, the balun is connected to a differential

probe jig with both probes connected to the center pins of two short sections of coaxial cable as shown in Figure 4.1. The jig is shown attached to a bazooka balun in Figure 4.2.

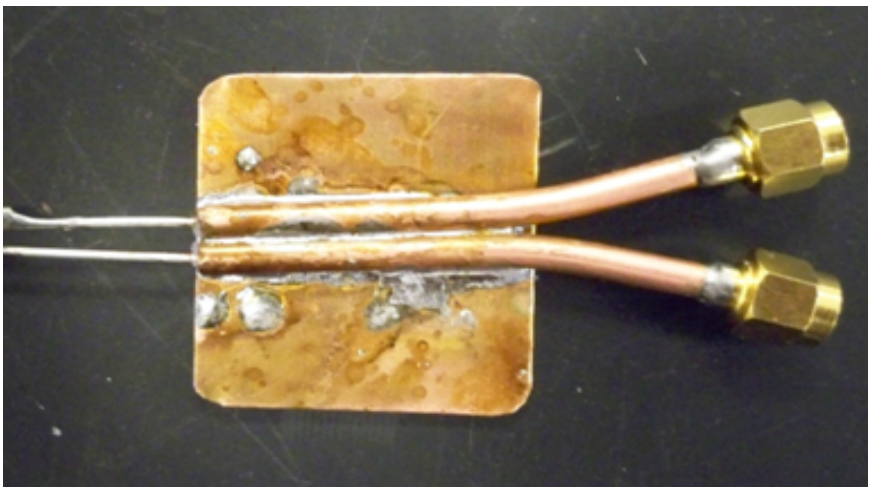

Figure 4.1: Balanced port measurement jig consisting of two probes fed to the center pins of two cables with a common ground

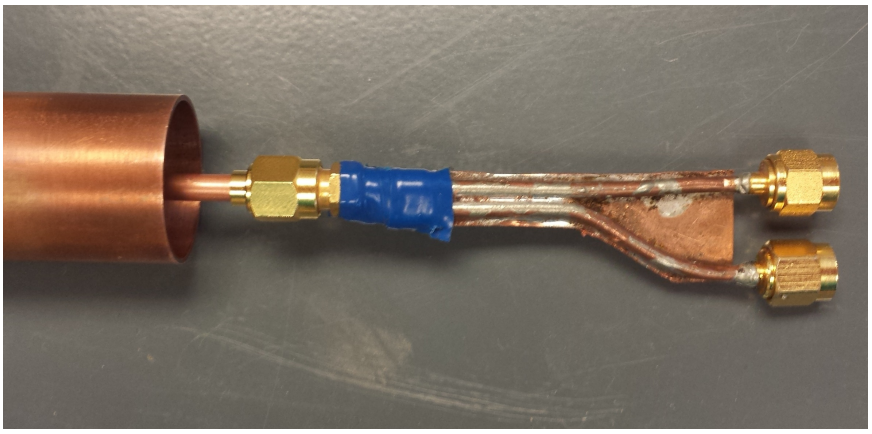

Figure 4.2: Balanced port measurement jig attached to a folded bazooka balun

Calculation of the CMRR requires two measurements. First, the network analyzer is calibrated to the ends of the test cable, and then an electrical delay is added to de-embed the measurement to the probe tips of the measurement jig [26]. Once de-embedded, S_{21} and S_{31} of the balun-jig system are measured individually, with the other port terminated in a 50 Ω load. Once S_{21} and S_{31} are known, the CMRR can be calculated by equations (4.1) through (4.3).

4.2 Quarter-Wavelength Balun

Figure 4.3 shows the bazooka balun design with $l = \lambda/4 = 214$ mm, operating at 350 MHz. The construction was straightforward since LC circuits within the balun were not necessary.

Figure 4.3: Bazooka balun at 350 MHz

Figure 4.4 shows the simulated and measured CMRR in a dB scale. The measures required to calculate the CMRR are shown in Figure 4.5. The S-parameters S_{21} and S_{31} were converted to mixed-mode S-parameters S_{d1} and S_{c1} in order to determine the CMRR.

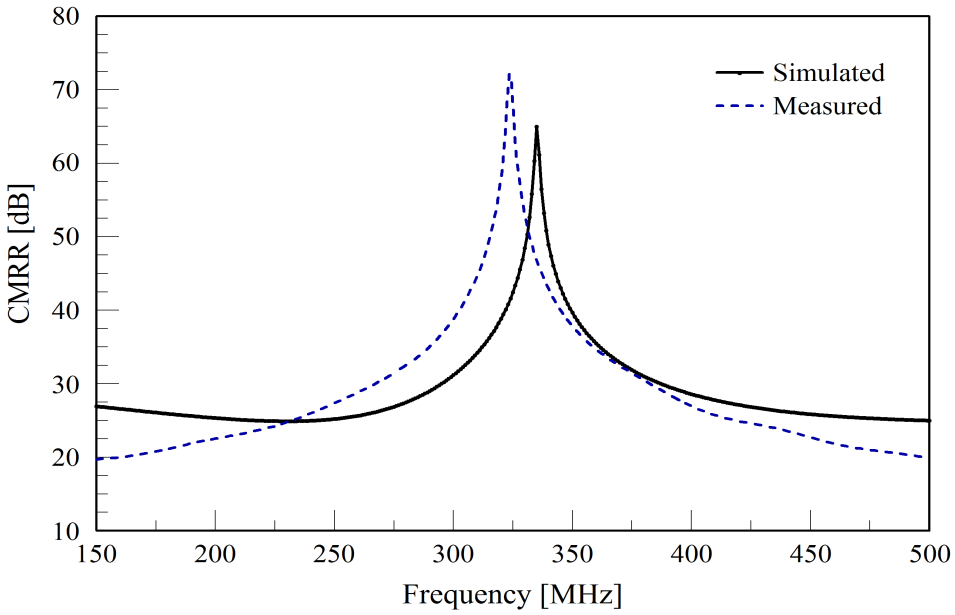

Figure 4.4: Bazooka balun measured and simulated data

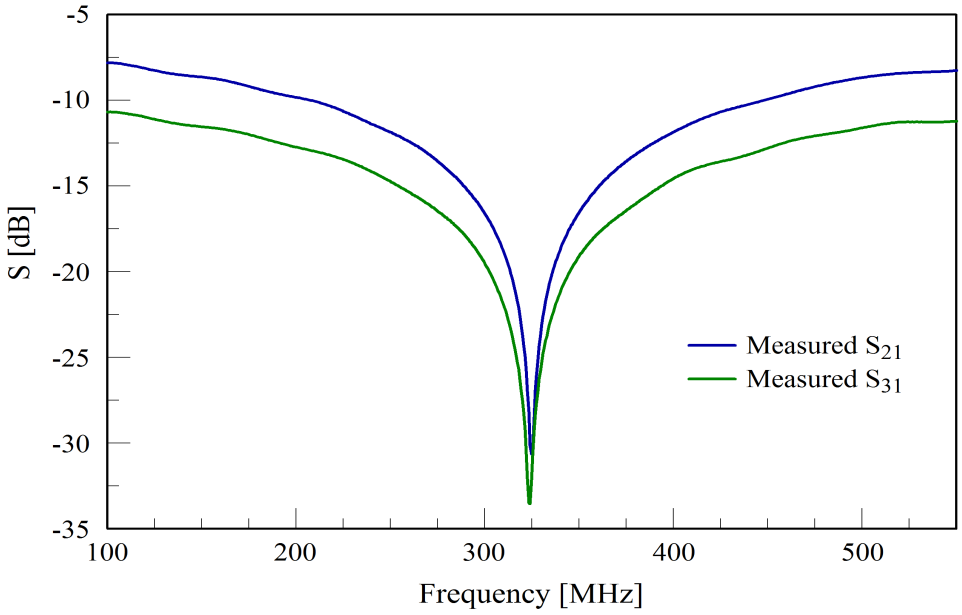

Figure 4.5: Bazooka balun measured S_{21} and S_{31}

Simulation and testing of the quarter-wavelength bazooka balun confirm that it is indeed operational to the corresponding $\lambda/4$ frequency. The simulated and measured results agreed in terms of bandwidth and common mode rejection values; however it can be seen from Figure 4.4 that the measured frequency is downshifted to 325 MHz while the simulated is only downshifted to 345 MHz. This frequency shift might be due to an electrical delay between the balun and the jig probe.

4.3 Two-Resonator Design

A structure was needed for the two- and four-resonator designs to mount the LC circuits within the balun. Circular disks were made in a single-sided PCB board with dielectric constant $\varepsilon_r = 2.20$ and thickness 0.062 in (1.57 mm). Rectangular copper shapes in the circle were designed to mount the LC components as shown in Figure 4.6(a) and Figure 4.6(b). To ensure an electrical contact of the LC circuit with the inner wall, circuits were mounted in a foam structure with copper tape strip on the side of each LC as shown in Figure 4.6(c) and Figure 4.6(d). The disks were placed in the coaxial cable at $\lambda/4$ according to their respective frequencies as shown in Figure 4.7. Finally, the coax cable with the circuit was inserted in the copper pipe.

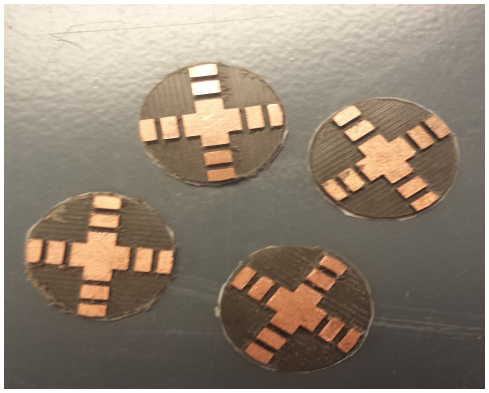

(a) Disks to mount the LC components

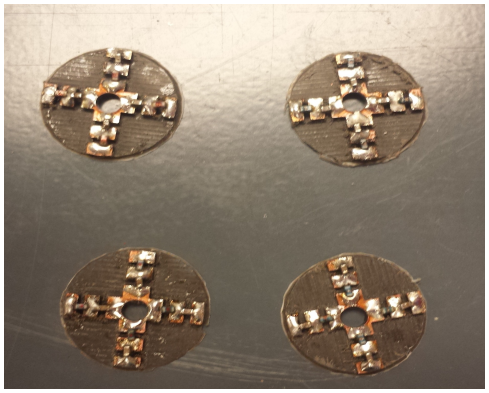

(b) Disk with LC components

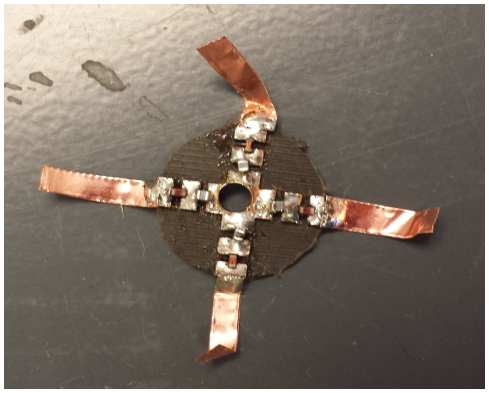

(c) Cooper tape to ensure electrical contact

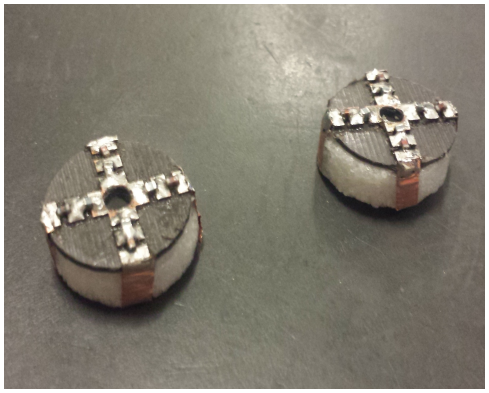

(d) Resonator Disk mounted in foam

Figure 4.6: LC circuits

Table 4.1 presents the LC circuit parameters in the design. The inductors' nominal values where chosen to be 64 nH and 30 nH with an inductance of

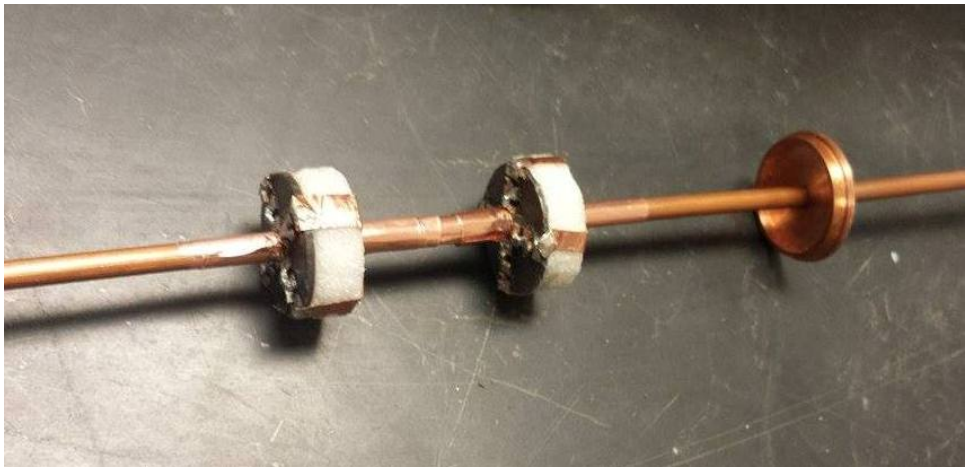

Figure 4.7: Two resonators spaced at $\lambda/4$

58.92 nH and 31.16 nH at their respective 512 MHz and 750 MHz frequencies. Capacitor values were calculated based on the inductance at the specified frequency and not at the nominal value. The resistance and bandwidth were calculated given the Q factor of the inductor in the data sheet. The resistance was not included in the physical model. It was used to account for losses introduced by the inductor. This resistance was used for simulation and analysis purposes.

Table 4.1: Two-Resonator Design

f_o **[MHz]**	**L [nH]**	**L at** f_o	**C [pF]**	**R** [Ω]	**Q**	**BW**
512	64	58.92	1.3	3.16	60	8.53
750	30	31.16	1.5	2.24	66	11.36

The CMRR was determined given the measured S_{21} and S_{31}. The CMRR response is shown in Figure 4.8(a). The measured S_{21} and S_{31} have different shapes and different S values as shown in Figure 4.8(b). The different shapes were not expected, in theory S_{21} and S_{31} have the same magnitude. This might be due to the performance of the probe jig. The S_{21} curve has three distinct peaks, whereas the S_{31} has one distinct peak close to 300 MHz. Since the CMRR is a vector algebraic operation, the result is a curve with a peak

at 280 MHz and smooth over the 350 to 850 range. Despite the fact that the magnitude of S_{21} is not equal to S_{31}, the performance of this balun is better than expected. The CMRR values are above 40 dB with a smooth response over a larger frequency range.

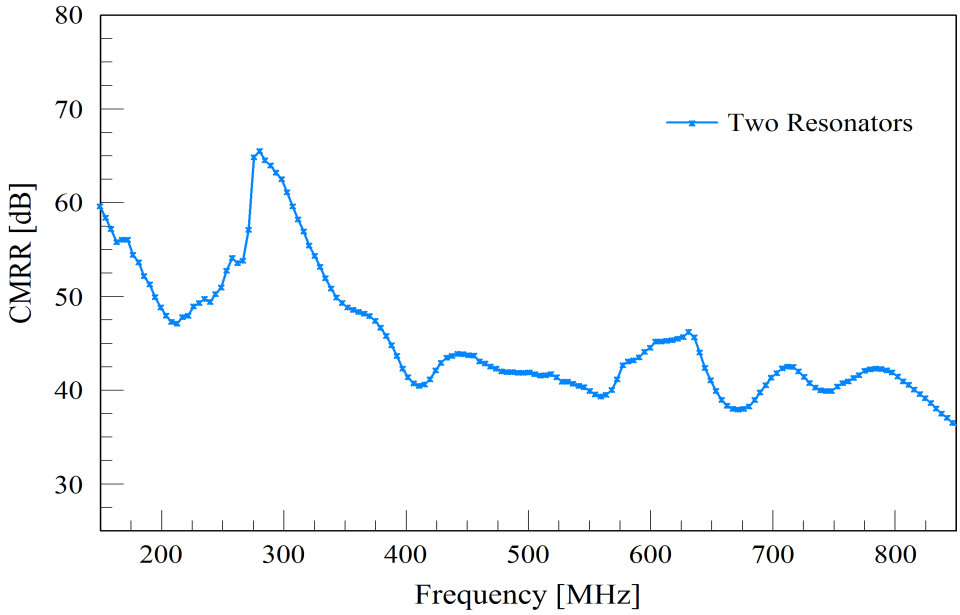

(a) CMRR two resonators

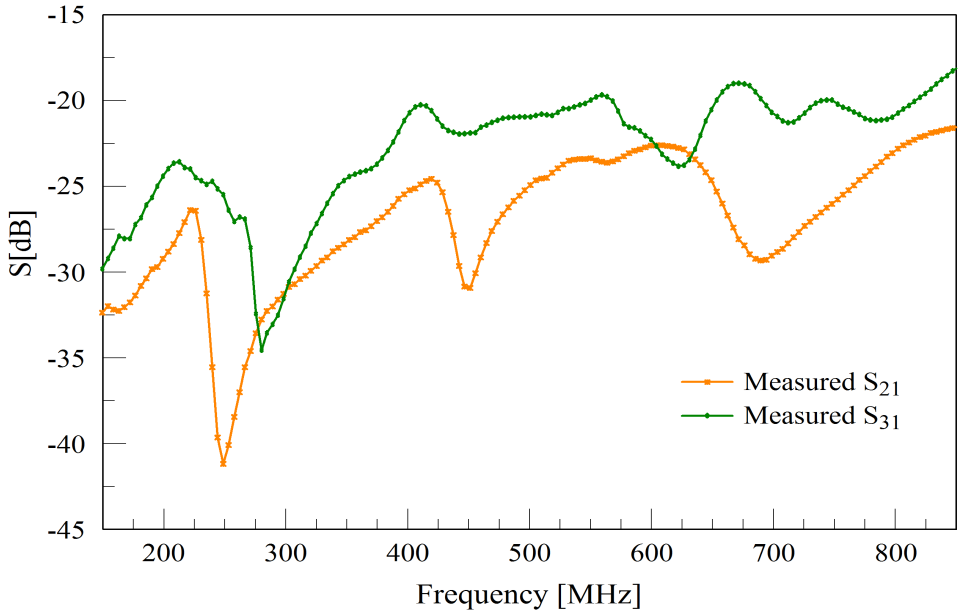

(b) Measured S_{21} and S_{31}

Figure 4.8: Results for the two-resonator design

4.4 Four-Resonator Design

The four LC circuits placed around the coaxial cable are presented Figure 4.9. This structure was placed in a copper pipe to complete the balun. The components of each LC circuit are recorded in Table 4.2. Each circuit has four inductors and four capacitors, so this design has 32 components in total, making the construction challenging and time-consuming.

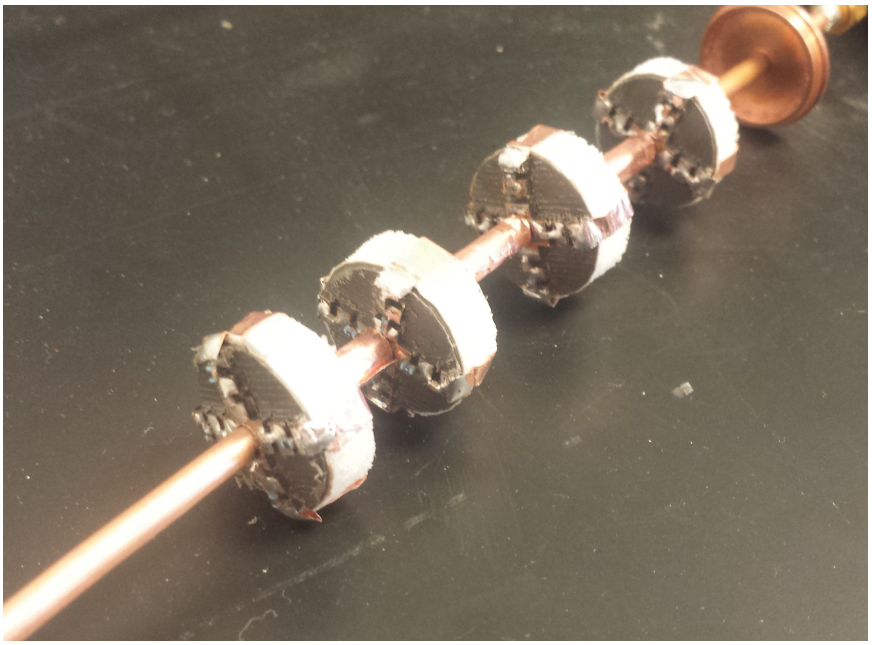

Figure 4.9: Four resonators spaced at $\lambda/4$

Table 4.2: Four-Resonator Design

f_o **[MHz]**	**L [nH]**	**L at** f_o	**C [pF]**	**R** [Ω]	**Q**	**BW**
423	68	70.13	2	3.51	53	7.98
512	56	55.52	1.8	2.86	63	8.12
620	33	33.76	2	2.10	62	10
750	30	31.16	1.5	2.24	66	11.36

The balun was measured, and the S_{21} and S_{31} are shown in Figure 4.11. Again, the parameters do not have the same magnitude. The CMRR given both measurements is presented in Figure 4.10. The response is smooth over a frequency range of 100 to 1000 MHz.

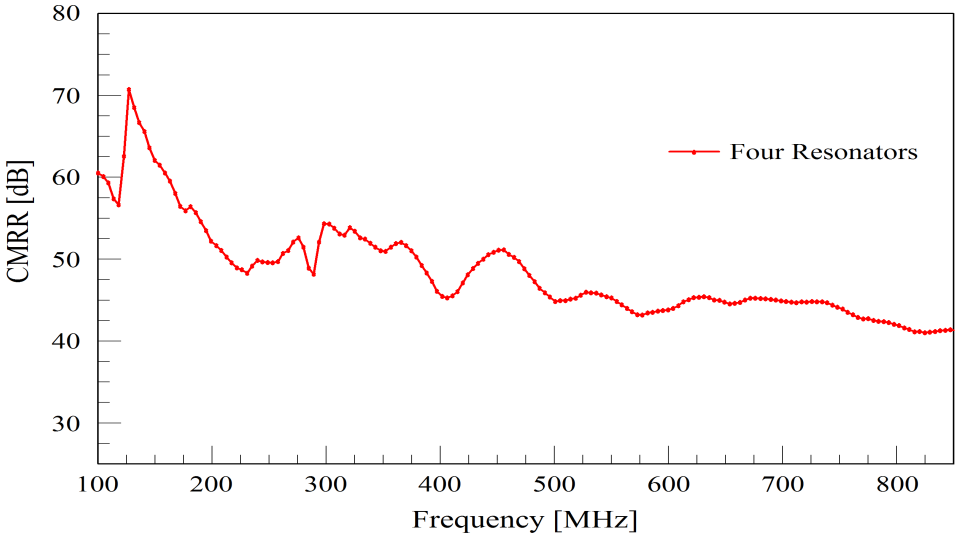

Figure 4.10: CMRR four resonators

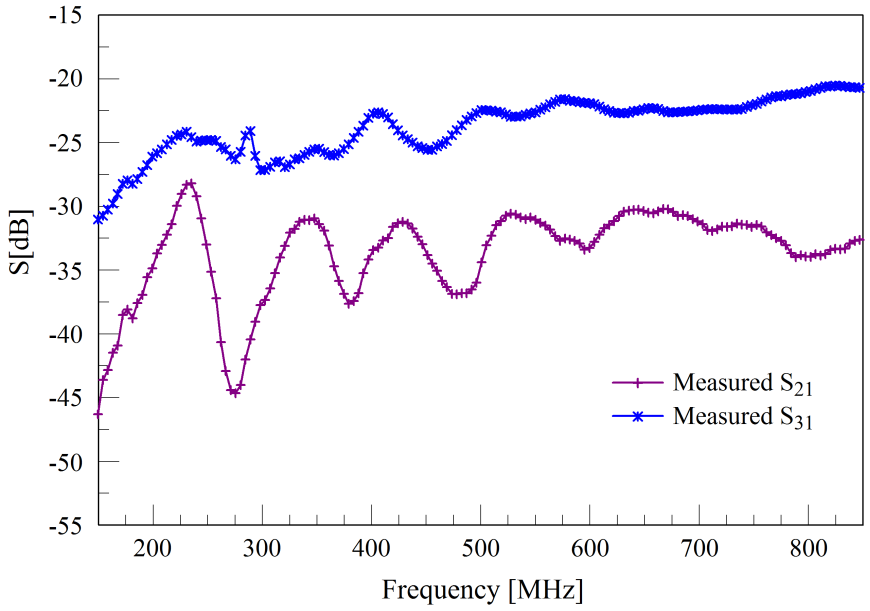

Figure 4.11: Measured four resonators

CHAPTER 5

CONCLUSIONS AND FUTURE WORK

5.1 Summary and Conclusions

The performance of the sleeve balun with series resonant LC circuit placed in a log-periodic manner has been studied. Different designs were investigated, taking into account the circuit placement and the quality factor Q. All simulations were consistent with theory. Simulation results demonstrated that the inductor quality factor Q affects the common mode rejection values. As expected, circuits with high Q values present high common mode rejection ratio with distinctive peaks close to the designed resonant frequency. Although high common mode rejection ratio was achieved, the response was not smooth over the frequency range. In contrast, resonant circuits with low Q factor, and therefore wide bandwidth, present a smoother response, but lower common mode rejection ratio.

In addition to simulations, three baluns were built and measured. The first balun was a quarter-wavelength design operating at one frequency. Simulated and measured results were consistent. The second balun consisted of two LC resonators at $f_o = 520$ MHz and $f_o = 750$ MHz. The third design had four LC circuits at $f_o = 423$ MHz, $f_o = 520$ MHz, $f_o = 620$ MHz and $f_o = 750$ MHz. Each resonant circuit was designed to have a 10 MHz bandwidth. Both baluns achieved a CMRR above 30 dB. A comparison of the CMRRs is shown in Figure 5.1. The balun with four LC circuits provides a smoother response with high CMRR values. The average CMRR for this design is 46.9 dB, while the average CMRR for the two-resonator design is 39.07 dB, over a frequency range between 100 MHz and 1000 MHz. Both designs are considered to have a good performance.

This response was not expected. Simulated designs with 10 MHz of bandwidth were less flat and with lower CMRR as shown in Figure 5.2. Despite the

fact that S_{31} was not as good as S_{21}, good CMRR values were achieved. Both designs have better than the simulated results and better performance than the single quarter-wavelength bazooka balun. The single quarter-wavelength bazooka balun can achieve good performance only at one frequency with values over 60 dB, but with a narrow bandwidth.

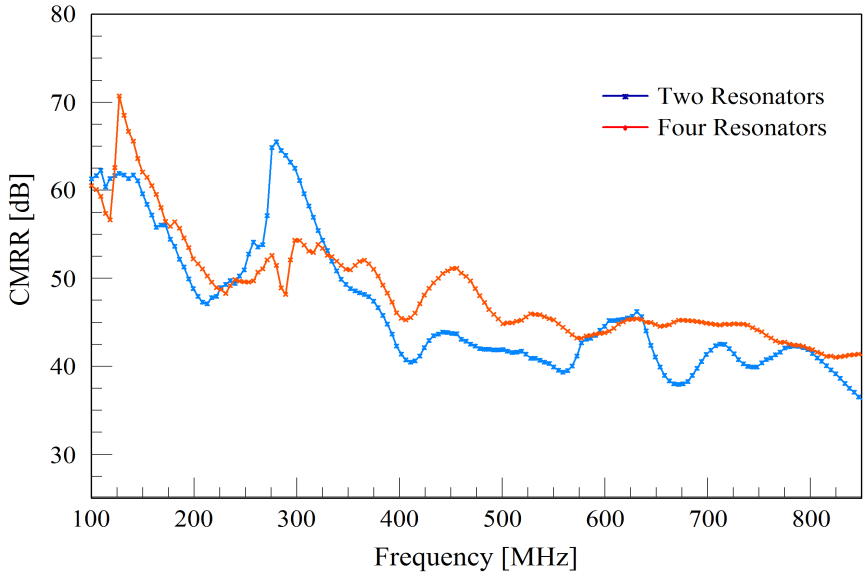

Figure 5.1: Comparison between the two designs

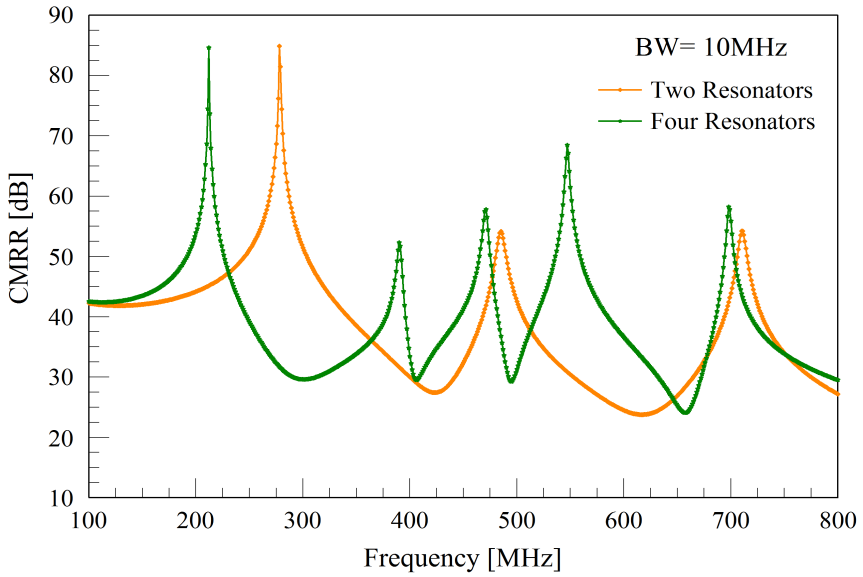

Figure 5.2: Simulations BW = 10 MHz for two- and four-resonator design

5.2 Future Work

In order to verify that the sleeve balun with series LC circuits has good performance, more research and work need to be done. The following points present some recommendations for future work.

- Build and replace the jig probe in order to repeat measurements: In theory, at the two differential terminals, the magnitudes of the signal are equal and opposite (180 ° phase shift). In our measurements S_{21} and S_{31} were not equal. This was due to the performance of the jig probe. A new probe needs to be built for a better system performance. Repeated measurements are needed to conclude that this balun indeed performs well.

- Antenna performance: A way to determine how well the balun can choke current over a range of frequencies is to attach an electrically small dipole antenna. Measurements and simulations of radiation patterns at different frequencies need to be explored.

- Investigate how the total impedance of the LC resonators affects the wide-band frequency range. In the designs of this work, the range in which the balun was supposed to perform well was between 350 MHz and 750 MHz; however, results show that the balun can perform well over a wider range. This effect might be due to the total LC impedance in the balun.

- Investigate a different range of frequencies with a different log periodic-period.

REFERENCES

[1] J. Bernhard, J. Adams, M. Anderson, and J. Martin, "Measuring electrically small antennas: Details and implications," in *Antenna Technology, 2009. iWAT 2009. IEEE International Workshop on*, March 2009, pp. 1–4.

[2] O. Staub, J. Zrcher, and A. Skrivervik, "Some considerations on the correct measurement of the gain and bandwidth of electrically small antennas," *Microw. Opt. Technol. Lett.*, vol. 17, no. 3, pp. 156–160, Feb. 1998.

[3] T. Koskinen, H. Rajagopalan, and Y. Rahmat-Samii, "Impedance measurements of various types of balanced antennas with the differential probe method," in *Antenna Technology, 2009. iWAT 2009. IEEE International Workshop on*, March 2009, pp. 1–4.

[4] R. Lawallen, "Baluns: What they do and how they do it," *QST*, vol. 1, pp. 157–163, Apr. 1985.

[5] J. Sevick, *Transmission Line Transformer*, 4th ed. New York, NY: SciTech Inc., 2001.

[6] B. Collins, "The operation and design of baluns," Oct. 2006, BCS & Associates Ltd., England. [Online]. Available: http://www.bscassociates.webspace.virginmedia.com/Bibliography/Paper-44.pdf

[7] T. Milligan, *Modern Antenna Design*, 2nd ed. Wiley-IEEE Press, 2005.

[8] R. Wallance, "Antenna selection guide," Texas Instruments, Dallas, TX, Tech. Rep. AN058, 2010.

[9] J. Sevick, *Understanding, Building, and Using Baluns and Ununs*. Hicksville, NY: CQ Communications, Inc., 2003.

[10] C. Balanis, *Antenna Theory*, 3rd ed. New York, NY: John Wiley and Sons, Inc., 2005.

[11] "My antennas," 2012. [Online]. Available: http://myantennas.com/wp/tech-info/about-baluns/

[12] B. Collins and S. Saario, "The use of baluns for measurements on antennas mounted on small groundplanes," in *Antenna Technology: Small Antennas and Novel Metamaterials, 2005. IWAT 2005. IEEE International Workshop on*, March 2005, pp. 266–269.

[13] B. Eggers, "An analysis of the balun," *QST*, pp. 19–21, Apr. 1980.

[14] D. Jorgesen and C. Marki, "A tutorial on baluns, balun transformers, magics-ts and 180 hybrids," Marki Microwave, Inc., Morgan Hill, CA, Tech. Rep., 2014.

[15] R. Li, *RF Circuit Design*, 2nd ed. Hoboken, NJ: John Wiley & Sons, Inc., 2012.

[16] C. Icheln, J. Krogerus, and P. Vainikainen, "Use of balun chokes in small-antenna radiation measurements," *IEEE Trans. Inst. Meas.*, vol. 53, no. 2, pp. 498–506, Apr. 2004.

[17] M. Slater, "Design and analysis of direction-of-arrival estimation systems using electrically small antenna arrays," Ph.D. dissertation, University of Illinois, Urbana-Champaign, IL, 2012.

[18] *Measurement techniques for Baluns*, Anaren Inc., East Syracuse, NY, 2005. [Online]. Available: https://www.anaren.com/sites/default/files/uploads/File/BalunTesting_0.pdf

[19] D. Bockelman and W. Eisenstadt, "Combined differential and common-mode scattering parameters: theory and simulation," *Microwave Theory and Techniques, IEEE Transactions on*, vol. 43, no. 7, pp. 1530–1539, Jul 1995.

[20] M. Slater and J. Bernhard, "Study of balun effects with electrically small antennas for a whitespace direction finding system," in *Antennas and Propagation Society International Symposium (APSURSI), 2010 IEEE*, July 2010, pp. 1–4.

[21] M. Basraoui and S. Prasad, "Wideband, planar, log-periodic balun," in *Microwave Symposium Digest, 1998 IEEE MTT-S International*, vol. 2, June 1998, pp. 785–788 vol.2.

[22] S.-H. Ye and C.-Y. Chen, "A symmetric log-periodic balun for ultra-wideband application," in *Electron Devices and Solid-State Circuits, 2007. EDSSC 2007. IEEE Conference on*, Dec 2007, pp. 741–743.

[23] K. Vinayagamoorthy, "Baluns, hybrids and power dividers for ultra-wideband antennas," M.S. thesis, Chalmers University of Technology, Goteborg, Sweden, 2012.

[24] D. Pozar, *Microwave Engineering*, 4th ed. New York, NY: John Wiley and Sons, Inc., 2011.

[25] S. Franke, *ECE 453 Wireless Communications Systems.* Champaign, IL: Self-published, 2010.

[26] "Investigating inductor requirements for power and microwave designs," Penton Media Inc., Tech. Rep., 2014.